UNIVERSITA' DEGLI STUDI DI TRIESTE

XX CICLO DEL

DOTTORATO DI RICERCA IN NANOTECNLOGIE

SPECTROSCOPIC PROCEDURE FOR *IN VIVO* DETECTION OF LIVER METASTASES IN A RAT MODEL

(Settore scientifico-disciplinare FIS/07 FISICA APPLICATA (A BIOLOGIA E MEDICINA))

DOTTORANDO

Francesco Trotta

COORDINATORE DEL COLLEGIO DEI DOCENTI

CHIAR.MO PROF. Maurizio Fermeglia

Università di Trieste

SUPERVISORE

DR. Massimo Tormen

Università di Trieste

TUTORE

DR. Ubaldo Prati

Fondazione Campanella
Centro per lo studio e la cura dei tumori
Centro Oncologico di Eccellenza - Catanzaro

ANNO ACCADEMICO 2007-2008

A Marco

TABLE OF CONTENTS

ABSTRACT

Recenti ricerche hanno messo in rilievo la possibilità di distinguere diverse tipologie di tessuti attraverso valutazioni bio-elettriche e meccaniche, ed in particolare di differenziare i tessuti sani dalle lesioni tumorali attraverso la misura di questi parametri.

Le metodiche spettroscopiche vanno inserite nel novero delle procedure di maggior interesse nel campo della definizione e della caratterizzazione tissutale (biopsia ottica); difatti, lo sviluppo e la disponibilità di strumenti ad elevata sensibilità ha permesso di ottenere risultati molto incoraggianti in diversi settori di applicazione (tumore della mammella, della cervice uterina, del tratto gastro-intestinale).

L'attività di ricerca è stata finalizzata alla realizzazione e alla validazione di un nanosenosore ottico in grado di discriminare tessuto epatico sano, tessuto fibro-connettivale e tessuto neoplastico in un modello di metastasi epatiche da carcinoma colico nel ratto.

Le metastasi epatiche sono state indotte in ratti BDIX mediante inoculo intrasplenico di cellule di carcinoma colico stabilizzate in coltura da ratti singenici [DHD/K12/Trb (PROb)]. L'inoculo delle cellule neoplastiche è stato effettuato dopo clampaggio del ramo portale mediano al fine di escludere dal flusso ematico (e dall'invasione neoplastica) i lobi epatici mediani: in questo modo, nello stesso ratto è stato possibile eseguire l'analisi spettroscopica sia del tessuto sano che del tessuto neoplastico con il vantaggio di ridurre al minimo la variabilità del campione.

Nel sistema di biopsia ottica adottato nel nostro progetto di ricerca la luce bianca proveniente da una lampada alogena attraversa un beam splitter e viene indirizzata al campione; la luce riflessa viene quindi inviata allo spettrofotometro e infine al computer per l'analisi matematica e statistica degli spettri ottenuti.

Per effettuare la diagnosi del tessuto sono state utilizzate le informazioni derivanti dalla cosiddetta "diffuse reflectance spectroscopy (DRS)" che fornisce una misura dell'assorbimento e dello scattering multiplo dei fotoni all'interno del tessuto: da questi dati si ottengono informazioni sia di tipo biochimico che morfologico del campione in esame.

Lo strumento è in grado di ottenere anche le informazioni provenienti da un'altra metodica, la "spettroscopia a scattering singolo", che si caratterizza per fornire informazioni di tipo geometrico-morfologico dello strato più superficiale sul tessuto analizzato, prendendo in considerazione solo i fotoni che interagiscono con lo strato a più immediato contatto con la sonda. Nonostante in una sessione preliminare di misura su tessuto artificiale (sferette di polistirene immerse in un liquido a densità ottica simile al citoplasma) queste ultime informazioni siano state ottenute, nelle successive sessioni *ex vivo* (fegato espiantato) e *in vivo* (fegato, tessuto peritoneale) la spettroscopia a scattering singolo non si è rilevata utile per la diagnosi.

Nell'analisi *ex vivo* sono state eseguite con lo strumento nella configurazione DRS 750 misure per il tessuto sano e 750 per il tessuto neoplastico. Gli spettri relativi a ciascun tessuto, dopo normalizzazione, sono stati confrontati e l'andamento delle

curve ha mostrato differenze che sono risultate, al test t-Student, statisticamente significative (livello di confidenza LC = 95%).

La buona accuratezza diagnostica del sistema è stata confermata dalla costante concordanza dei risultati dell'analisi spettroscopica con l'esame istologico effettuato su aree corrispondenti.

Nella sessione *in vivo* (500 misure per ciascun tipo di tessuto) i risultati sono stati paragonabili a quanto evidenziato dallo studio *ex vivo*: anche in questo caso sia la validazione statistica (test t-Student con LC = 95%) sia la corrispondenza tra analisi spettroscopica ed esame istologico di aree corrispondenti hanno confermato l'elevata accuratezza diagnostica dello strumento.

Infine, è stato presa in considerazione la diagnosi del tessuto connettivo (500 misure anche in questo caso) che presenta caratteristiche macroscopiche molto simili al tessuto neoplastico e la cui differenziazione risulta particolarmente importante in ambito clinico.

Anche in questo contesto i risultati sono stati incoraggianti e confermati dalla validazione statistica e dall'esame istologico.

Dai risultati ottenuti si può evincere la buona accuratezza diagnostica del sistema nei confronti dei vari tipi di tessuto (fegato, tessuto connettivale, tessuto neoplastico). Questa caratteristica, associata alla capacità dello strumento di fornire risultati in tempo reale, porrebbe le basi per una successiva valutazione dello strumento in ambito clinico-chirurgico in vista di un uso intra-operatorio.

INTRODUCTION

Biological tissue is assumed to behave as a turbid optical medium (1, 2). Several components are considered as responsible for both the absorption and the scattering of an incident light radiation (3). The latter phenomenon provides significant attractiveness as far as the field of the optical biopsy is concerned, mainly due to the possibility of investigating tissue pathologies, such as cancerous or even pre-cancerous lesions, by means of a non-invasive approach.

It is generally assumed that changes in the optical properties of biological tissues are the consequence of variations involving either the physiology or the morphology of the cells (4).

In the field of tissue characterization two spectroscopic approaches showed interesting results: the diffuse reflectance spectroscopy (DRS) (4) and the light scattering spectroscopy (LSS) (3, 5).

DRS collects information from multiple photon scattering inside the tissue, while, the LSS detects information from single photon scattering after light interaction with the most superficial cellular layer. In fig. 1 the different phenomenology of DRS and LSS is shown.

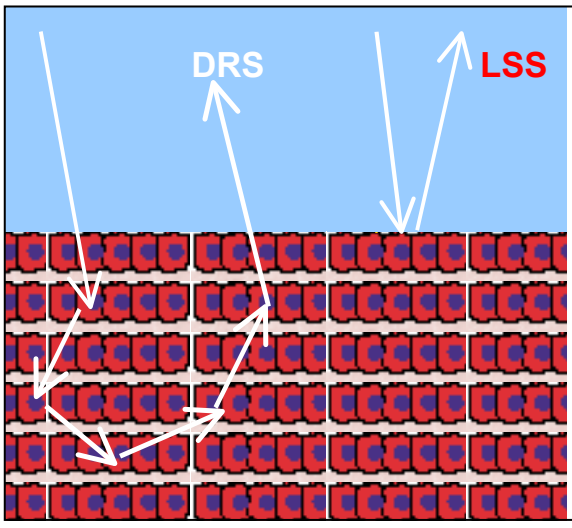

Fig 1. DRS and LSS phenomenology.

Thus, while DRS provides biochemical and morphological information of a considerable volume of tissue, LSS provides information of geometry and morphology of the cellular layer closest to the scanning probe.

Several recent studies, aimed at the achievement of consistent solutions for the equations derived from the complex theories concerning the LSS, have been especially focussing on the measurements of the optical properties within the superficial layers of the biological tissue, for example at the level of mucosae (3). As a matter of fact, many types of solid tumours arise within the epithelial layers and some common features have been reported, mostly concerning the morphology and the invasiveness of the malignant cells in the underlying tissues. The evidence of a significant enlargement of the nuclear dimensions in the tumour cells and cells crowding, as compared with those of the normal tissue, was obtained first through optical microscopy, the gold-standard technique, as reported for example in the case of breast, colon, bladder, prostate, cervix and liver cancers (5).

The equation proposed by Van de Hulst (6) has been used in order to describe the optical scattering cross-section (σ) of the epithelial nuclei and the related reflectance (R), as measured by means of an optical probe and conformingly to the theory of Mie (3).

By means of such analysis it has been possible to differentiate effectively the nuclear size distribution of malignant cell lines from that of the normal counterpart (nuclear size of neoplastic cells appears larger than normal) (Fig.2)

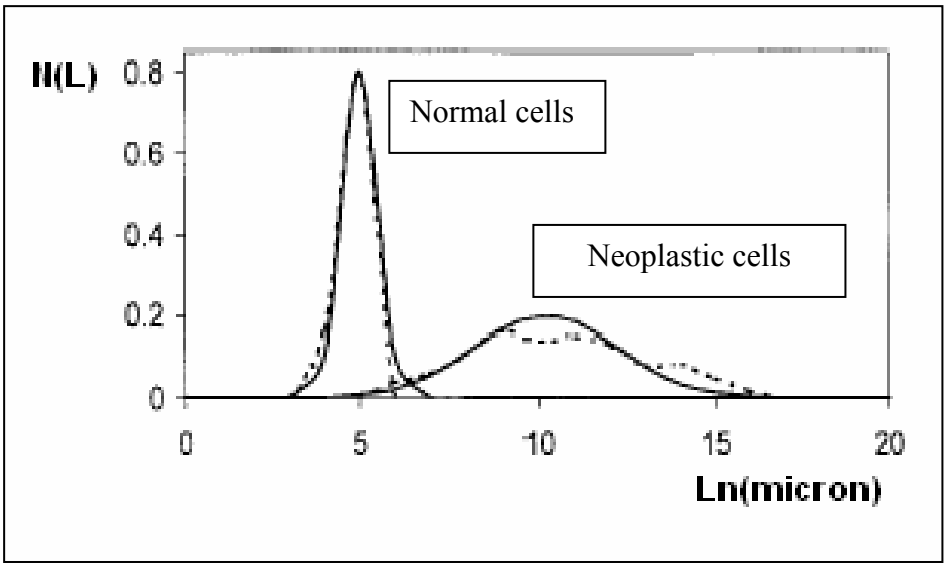

Fig. 2. Nuclear size distribution N(L) of normal and neoplastic cells (colon cell line).
Continuous line: nuclear size as measured by means of LSS; dotted line: nuclear size as measured by means of optical microscopy.

Unfortunately, other sub-cellular structures of minor dimensions, ranging from the mitochondrion to the collagen based extracellular matrix, and including several chromophores such as the haemoglobin, contribute significantly to the scattering or absorption of the light (3), so that the averaged scattering properties in a tissue depend ultimately on the individual scattering properties of such sub-cellular entities and their relative concentrations, yet the prediction of each sub-cellular particle's size contribution to the transport scattering coefficient (μ'_s) remains a controversial item (7, 8). For example, in the study of Beauvoit and collaborators

(9) a correlation has been shown between μ'_s and the mitochondrial content of a panel of rat's investigated tissues, the white adipose tissue representing an intriguing case, since the transport scattering coefficient was consistently high despite no correlation was observed with the content of the mitochondrial proteins. Such anomaly was explained by assuming that the high content of lipid particles in this anatomical district could be the main responsible for the scattering effect. Moreover, in a subsequent report (10), where analogous experiments were specifically performed in the rat liver, it is claimed that the mitochondria rather than the nuclei are the main scattering centres. In spite of the discrepancies emerging from the conclusions regarding the identification of the scattering centres, the LSS was proposed as a valid methodology for distinguishing the dysplasia and the cancer from the normal tissue or other benign conditions (11-13), its use being claimed as little or non-invasive and suitable for providing real-time results. For example, LSS based techniques were applied at a clinical level for the breast cancer diagnosis (14).

Beside such approaches, the differential path length spectroscopy (DPS) – a technique similar to DRS - has been validated for the diagnosis of several tumour types (4).

The basic instrumentation required for such analysis is analogous to that necessary in order to investigate the biological samples by means of LSS and proposed by Amelink and collaborators, although the probe's configuration is different (15).

In particular, we have used the latter configuration in order to analyse the DRS signal acquired from the liver, LSS signal being not detectable in our model (see Results and Discussion).

The instrument capability of detecting the metastatic lesions was assessed in a rat model. The metastases were induced by an intra-splenic inoculation of a colon carcinoma derived cell line, specifically affecting the right lobes of the liver, while leaving the left portion of the same organ unaffected and therefore useful as an internal control aimed at reducing the experimental variability. Such procedure allowed for the identification of diagnostic wavelength intervals in the visible range, on the basis of differences clearly detectable either from the reflectance intensities or the spectra profiles. The analytical approach was validated through statistical tests that provided a confidence level (c. l.) $\geq 95\%$.

The discriminatory capability of our probe could rely either on macroscopic characteristic of the specimens such as the colour, or on the peculiarities of several candidate sub-cellular structures, yet to be identified.

In any case such results appear encouraging for continuing the assessment of the diagnostic capability beyond the preclinical level.

AIM

This research project focuses on the validation of a diffuse reflectance spectroscopy-based system for discriminating the healthy liver and the connective tissue from the colorectal liver metastases in a rat model.

MATERIALS AND METHODS

Induction of liver metastases

A total of 125 male BDIX rats, weighing 250-300 g, were used and treated according to the local authority's guidelines.

The surgical procedures were performed under general anaesthesia by intramuscular injection of Tiletamine and Zolazepam 8 mg/kg each (ZOLETIL).

Liver metastases were induced by intra-splenic injection of neoplastic cells of a colon cancer cell line [DHD/K12/Trb (PROb)] (16).

In anaesthetized animals a midline or trasverse laparotomy was performed, the spleen was isolated and the portal branch directed to the left lateral lobe (LLL) and the left medial lobe (LM) was clamped (fig. 1) in order to exclude them from blood inflow.

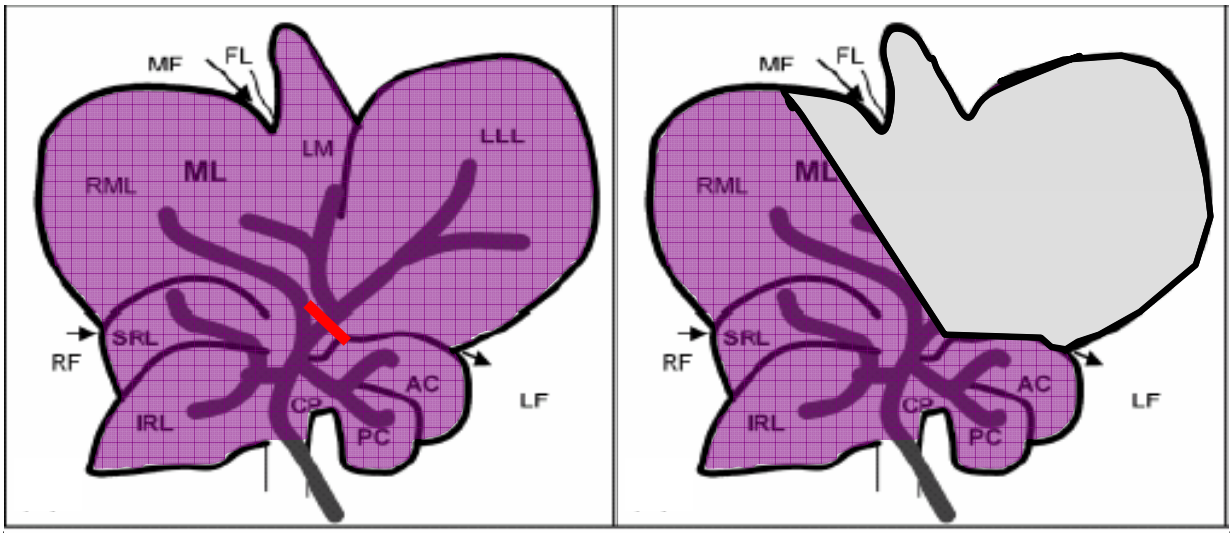

Fig. 1. Rat liver and portal vein branches.

Left: Red line represents the site of portal clamping (portal branch to left lateral lobe (LLL) and left medial lobe (LM).
Right: Grey area represents the lobes excluded from blood inflow (LLL and LM, not susceptible to metastatic implants); the remaining lobes are susceptible to metastatic implants (see text and fig.3).

IRL: inferior right lateral lobe, SRL: superior right lateral lobe, RML: right medial lobe, ML: median lobe, RML: right portion of the medial lobe, LM: left portion of the medial lobe, LLL: left lateral lobe, CP: caudate process, AC: anterior caudate lobe, PC: posterior caudate lobe.

(From P. N. A. Martins and P. Neuhaus, Liver International 2007; courtesy of the authors)

Then 2 x 10^7 neoplastic cells were injected into the spleen through a 25 G needle (fig. 2).

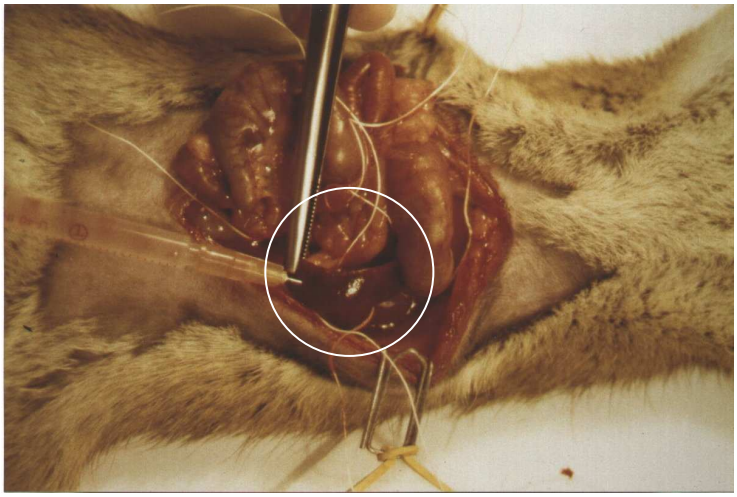

Fig. 2. Intra-splenic injection of neoplastic cells.

Upon transverse laparotomy, spleen isolation and portal clamping, the injection is performed.

The neoplastic cells invaded the right lobe, the right medial lobe and the caudate lobe only, while the remaining lobes (LLL and LM) were excluded from the blood inflow (due to the clamped portal branch). Thus, in the same organ both healthy and neoplastic areas were present (fig. 3), so that the same animal could be used for recording the spectra of the metastases as well as the spectra of the healthy tissue. Upon infusion, the splenic vessels were ligated and the portal clamp removed. Splenectomy was performed and the abdominal wall sutured (17).

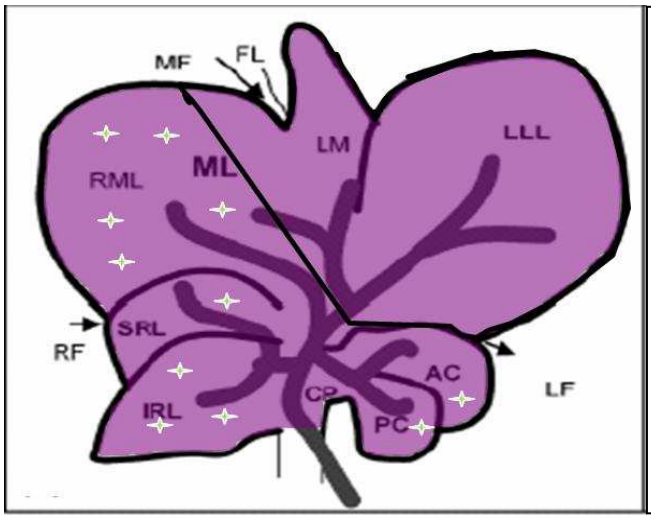

Fig. 3. Rat liver after injection of neoplastic cells.

White stars represent liver metastases: due to portal clamping left lateral lobe (LLL) and left medial lobe (LM) were not colonized by neoplastic cells.

IRL: inferior right lateral lobe, SRL: superior right lateral lobe, RML: right medial lobe, ML median lobe, RML: right portion of the medial lobe, LM: left portion of the medial lobe, LLL: left lateral lobe, CP: caudate process, AC: anterior caudate lobe, PC: posterior caudate lobe.
(From P. N. A. Martins and P. Neuhaus, Liver International 2007; courtesy of the authors)

Ten days after the surgical intervention metastatic nodules were macroscopically evident as compared to healthy tissue (fig. 4).

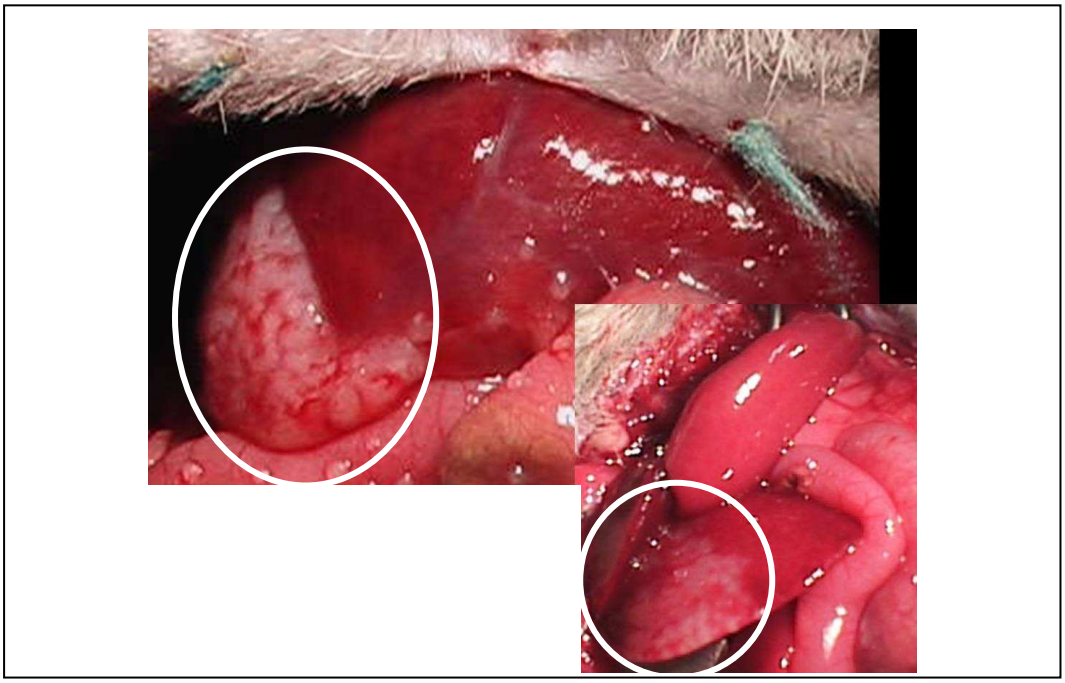

Fig. 4. Colorectal liver metastases.

Healthy liver appears purple; neoplastic nodules are indicated by white circles.

Spectroscopic analysis

As a first step the *ex vivo* analysis was performed.

Ten days after the metastases induction, the liver was explanted and the organ was scanned with the probe (fig.5).

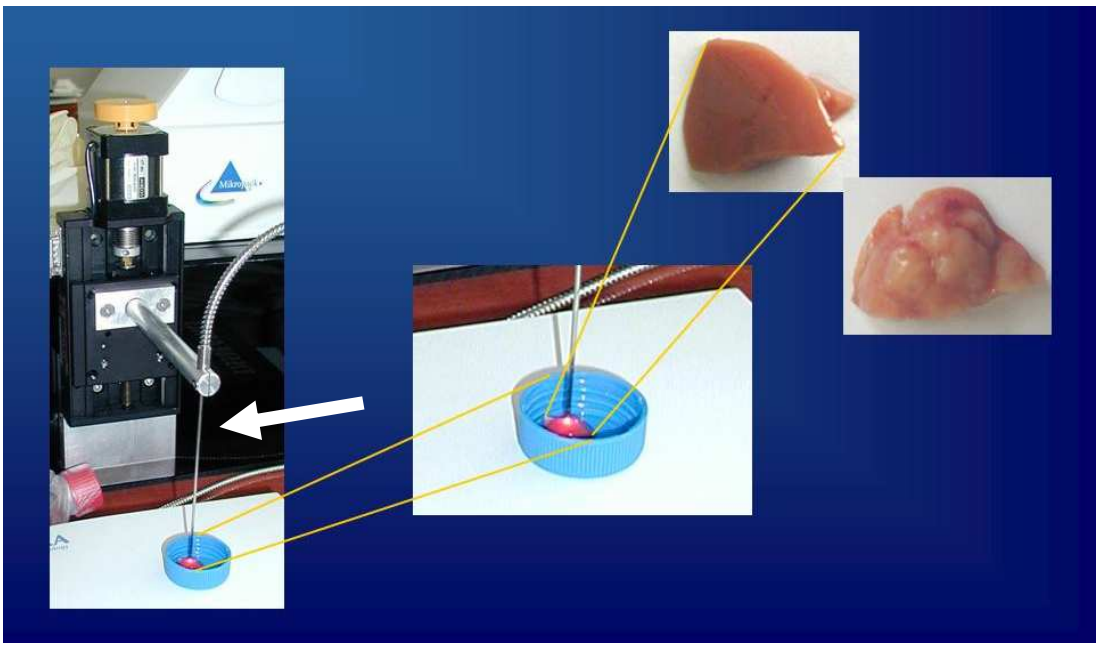

Fig. 5. *Ex vivo* spectroscopic analysis of rat liver.
Left panel: the probe positioning and tissue scanning (white arrow: probe) of the healthy tissue (top right).
The rightmost panel shows massive liver metastasis.

For the *in vivo* session the spectroscopic analysis was performed on the liver and the peritoneal tissue of anaesthetized rats (fig. 6).

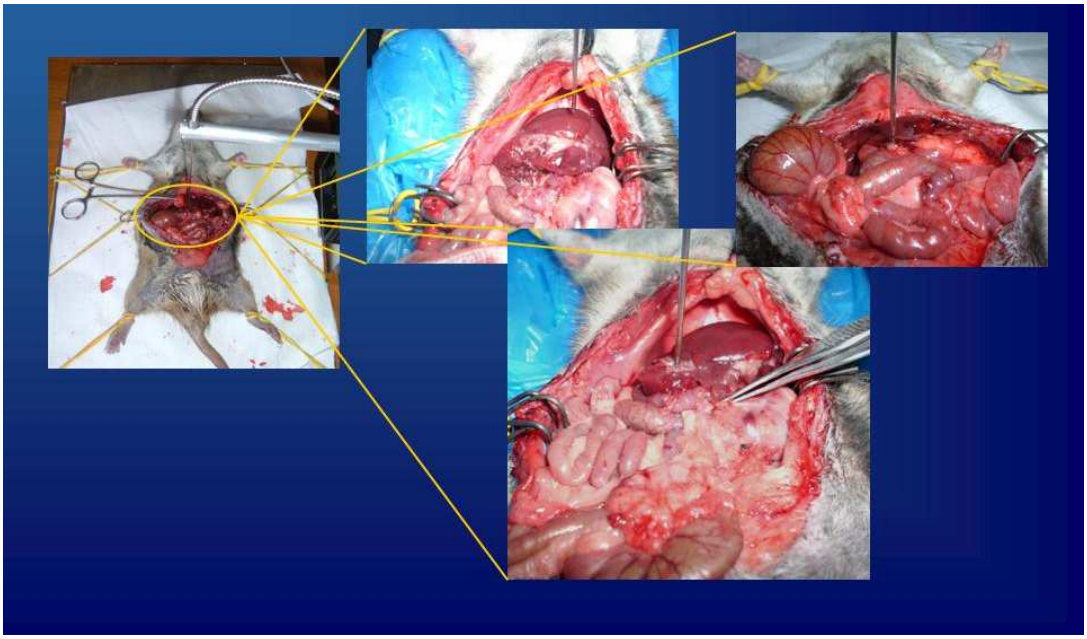

Fig. 6. *In vivo* spectroscopic analysis.
From left to right: laparotomy and probe positioning, analysis of healthy liver, of peritoneal nodule (connective tissue), of liver metastasis (bottom).

Then, the scanned tissues were prepared for pathologic examination (hematoxylin-eosin staining (18), magnification: 4 and 10 x) in order to confirm the correctness of the diagnosis.

For the *ex vivo* session 75 rats were used; 10 spectra from each rat were recorded from both healthy liver and metastases, for a total of 750 spectra per each experimental condition (healthy, tumour).

For the *in vivo* session 50 rats were used, providing a total of 500 spectra recorded from the healthy liver, the metastases and the peritoneal tissue (connective), respectively.

Due to statistical reasons, the 10 spectra included in each group (75 "healthy liver *ex vivo"*, 75 "metastasis *ex vivo"*, 50 "healthy liver *in vivo"*, 50 "metastasis *in vivo"*, 50 "connective tissue *in vivo")* were filed by means of progressive numbers so that a random number generator was then used for choosing one representative spectrum of each specific session (*ex vivo, in vivo*) per each animal and per each experimental condition (healthy liver, metastasis, connective tissue). Therefore the data presented are the average obtained from 25 independent measurements for a given experimental condition.

Instrumentation and configuration of the device

The instrumentation/configuration of the device are as those described by Amelink (15).

An halogen source (Mikropack HL-2000-FHSA) generates light (360 - 2000 nm), that passes through a polarizer and a 50/50 beam splitter before entering the delivery/collection fiber (core of 400 μm). The light reflected from the sample is directed toward the 'slave' channel of the spectrometer through the collection fiber (DRS signal). The reflected light entering the delivery/collection fiber (DRS-LSS signal) passes through the beam splitter and is then directed toward the 'master' channel of a dual channel spectrophotometer (Ocean Optics SD 2000) (fig. 7).

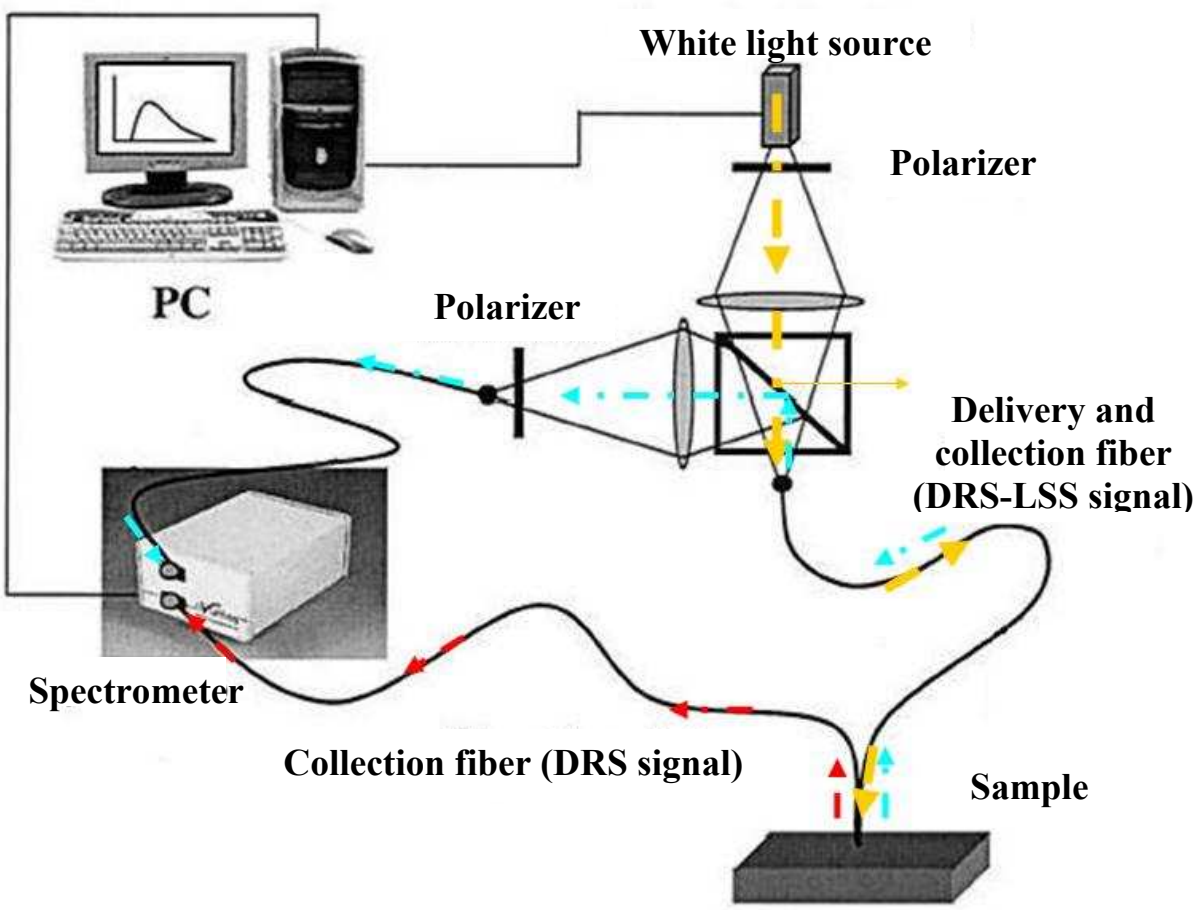

Fig. 7. Configuration of the device. The path of light directed toward the sample (yellow) and the reflected light directed toward the spectrophotometer ('slave' channel, in red) through the collection fiber is evidenced (DRS signal). Part of the signal was also directed to the spectrophotometer through the delivery-and-collection fiber, the beam splitter and the polarizer ("master" channel, in light blue, DRS-LSS signal). The LSS signal results from the difference between "master" and "slave" channels.

In the case of the DRS configuration the signal is directed toward the collection fiber connected to the "slave" channel of the spectrometer.

Instead, for LSS configuration the signal is acquired through the delivery/collection fiber connected to the "master" channel of the spectrometer. This signal contains both LSS and DRS information, respectively: thus, the pure LSS signal results from the difference between the "master" and the "slave" channels.

The probe consists of a metal tube (diameter 1.5 mm) containing 7 optical fibers (diameter 200 μm each), 6 for illumination and 1 for reading (fig. 8).

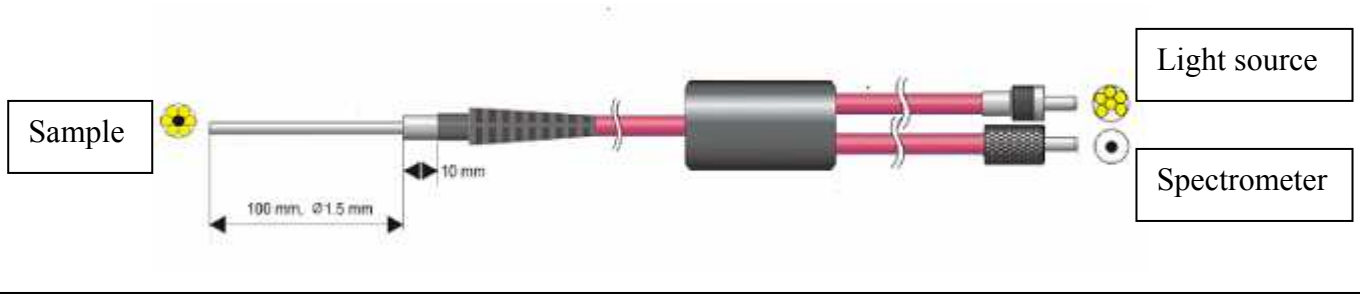

Fig. 8. The probe.
The light passes through the 6 illumination fibers, is directed to the sample and then to the spectrophotometer through the reading fiber.

The relevant wavelength range for these studies is within 450-900 nm (including the visible range).

The data acquisition process is controlled by a PC, as well as the positioning of the probe, obtained through a linear motor positioning stage.

Each acquired spectrum corresponds to one file, coding for a (1418×2) matrix, that was analysed through a dedicated MatLab code.

The data providing the dark (d) and the white reference (ref) spectral intensities, respectively, were acquired according to the spectrophotometer manufacturer's instructions (Ocean Optics) so that the reflectance (R) could be determined by the formula: $R = \frac{S - d}{ref - d}$, being S the spectral intensity read by the spectrophotometer for a given acquisition. Each acquisition consisted of data that were subsequently corrected by considering the "dark" (*d*) and the "white" (*ref.*) reference spectra, respectively: in the former case the signal resulted from the blocking of the path of the light in correspondence of the probe's tip, while in the latter situation a spectrally flat reflectance was produced by means of a standard surface. For each spectrum, the values of *S* and *ref* had been preliminarily normalized by the respective underlying area and MatLab was used in order to create simple codes for the normalization, as well as for the statistical analysis of the data and for drawing the diagrams at a resolution of 0,36 nm. The approximation of the first derivative was obtained by means of the function 'diff' included in the software. Beyond the calculation of the standard deviation, the mean values were subsequently compared by means of the t-Student test (non paired data, two tailed) and the Mann-Whitney test (non-directional), respectively.

Preliminary test of LSS configuration

In order to explore the instrument capability of detecting LSS signal (i.e. for assessing the cellular nuclear size), spectra from tissue phantom consisting of a solution of polystyrene spheres were recorded and the correct diameter of the beads (mimicking nuclei) was calculated (fig. 9).

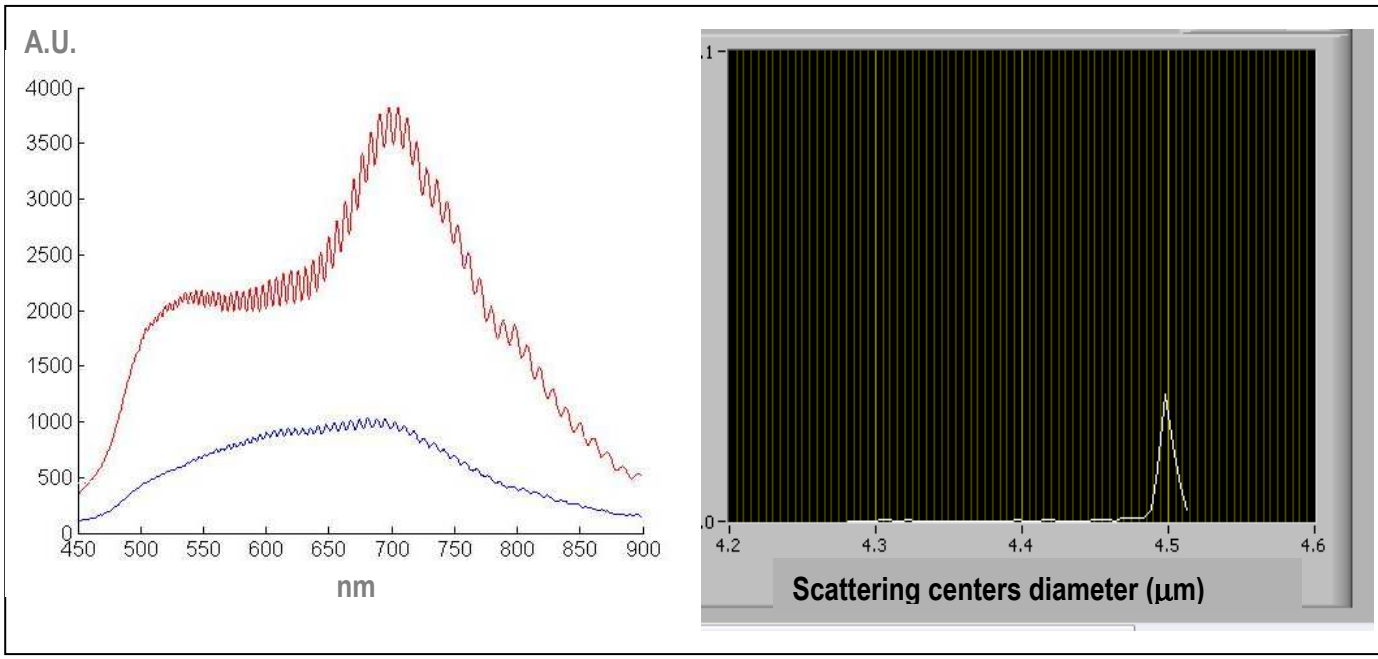

Fig. 9. An example of spectra showing the Mie scattering generated by a solution of microspheres of 4,5 µm in diameter. The profile in red is the recorded signal of the 'slave' channel of the spectrophotometer (DRS signal), whereas the profile in blue is the signal of the 'master' channel (DRS-LSS signal). [See fig .7]. Both signals are conveyed to the Fourier-transform procedure in order to measure the diameter of the beads shown n the right panel. A.U.: arbitrary units.

RESULTS

DRS CONFIGURATION

Ex vivo analysis

As indicated in Materials and Methods, sets of 10 spectra for the healthy and the metastatic tissue were collected respectively from explanted liver of 75 rats.

Twenty-five spectra (from a total of 750 spectra), representative for each experimental condition (normal and neoplastic tissue), were randomly chosen, normalised by the area included below the respective profile and mediated (fig. 1).

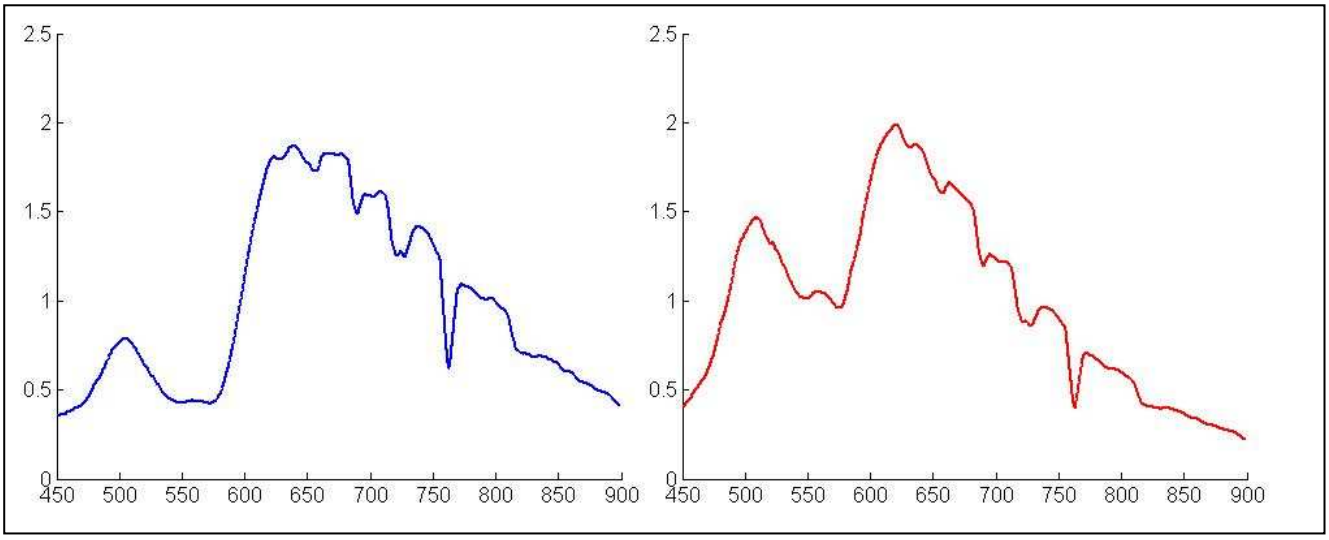

Fig. 1. The 'average' spectra obtained after *ex vivo* measurements of healthy liver (blue) and the metastatic counterpart (red).
Horizontal axis: wavelength values in nm; vertical axis: reflectance intensity expressed in arbitrary units.

In fig. 2 the ‘average’ spectrum for a given situation is presented with the standard deviation.

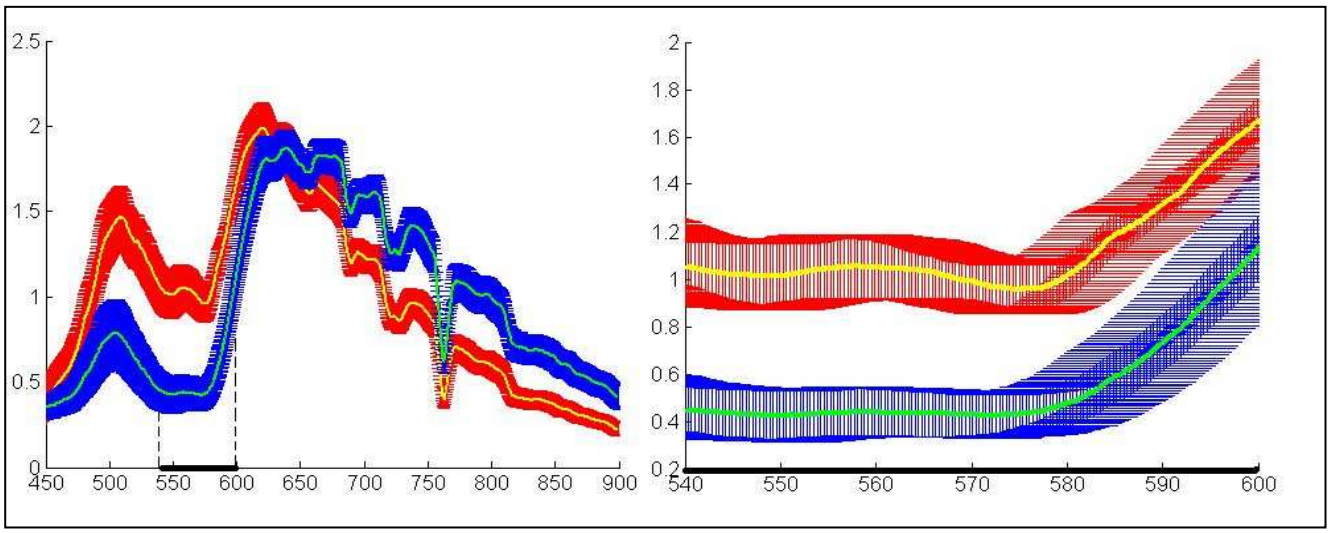

Fig. 2. Left: The average spectra shown in fig. 1 are merged and the standard deviation shown. Blue: liver; red: metastasis.
Right: The enlargement of the horizontal scale in the 540 ÷ 600 nm interval is shown in order to highlight the different trends.
Horizontal axis: wavelength values in nm; vertical axis: reflectance intensity expressed in arbitrary units.

Since each spectrum had been preliminarily normalised by the area included below the respective profile, the possibility that the observed differences between the metastasis and the healthy tissue could arise mainly from external physical factors, such as, for example, a variable distance between the sample and the probe’s tip during each measurement, or a variable intensity of the light directed toward each sample, rather than the molecular peculiarities and other characteristics specific for each anatomical district, resulted minimised.

Upon the data acquisition and normalization, two analytical approaches were subjected to the statistical validation.

The former was focussing on the differences between the reflectance intensities, as

recorded at specific wavelength's intervals for each kind of tissue, respectively. This approach revealed consistent differences in broad intervals: 500 ÷ 590 nm and wavelengths above 685 nm (fig. 2).

Another kind of information is provided by the approximation of the first derivative of the curves (fig. 3a-b), obtained thanks to the differentiation procedure provided by the software MatLab, and highlighting the characteristic shape of each 'average' spectrum shown in fig. 1.

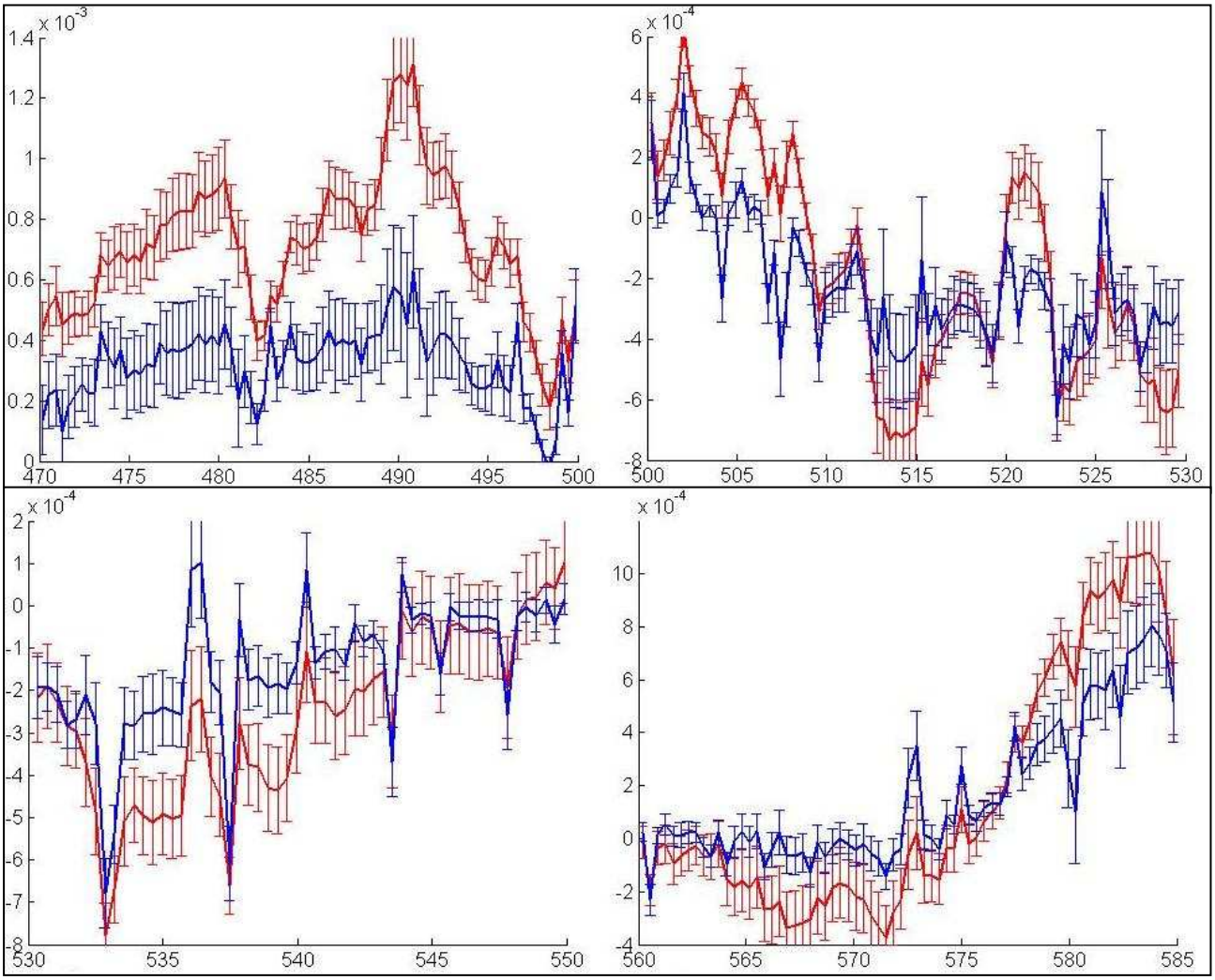

Fig. 3a. Comparison of (the approximation of) the first derivative of the curves shown in fig. 2. Blue: liver; red: metastasis. Wavelength interval: 470 – 585 nm.
Horizontal axis: wavelength values in nm; vertical axis (exponential factors arise from the scaling of the diagrams): 'slope' of the respective part of the diagram shown in fig. 2.
Values above 0 correlate with ascending values of the reflectance, values below 0 correlate with descending values, while 0 indicates flat portions of the spectrum.

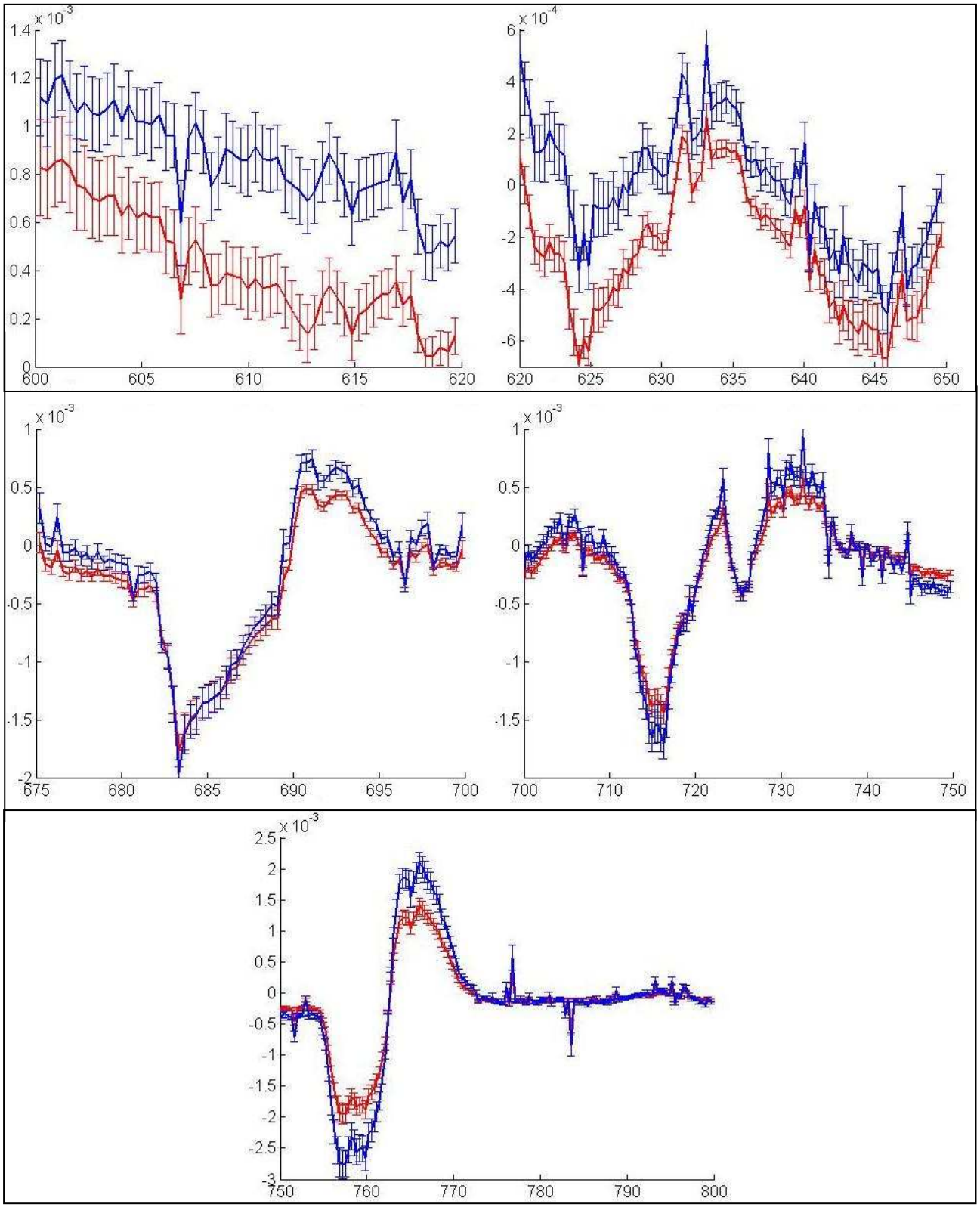

Fig. 3b. Comparison of (the approximation of) the first derivative of the curves shown in fig. 2. Blue: liver; red: metastasis. Wavelength interval: 600 – 800 nm.
Horizontal axis: wavelength values in nm; vertical axis (exponential factors arise from the scaling of the diagrams): 'slope' of the respective part of the diagram shown in fig. 2.
Values above 0 correlate with ascending values of the reflectance, values below 0 correlate with descending values, while 0 indicates flat portions of the spectrum.

This approach resulted in the elucidation of several and relatively large wavelength intervals where the two tissues can be discriminated, with a confidence level (c. l.) ≥ 95% for all the points of each interval, according to the t-Student and Mann-Whitney tests.

The pathologic analysis of each tissue sample confirmed the different typology of the tissues, therefore the differences evidenced by the respective spectra result consistent with this observation (fig. 4).

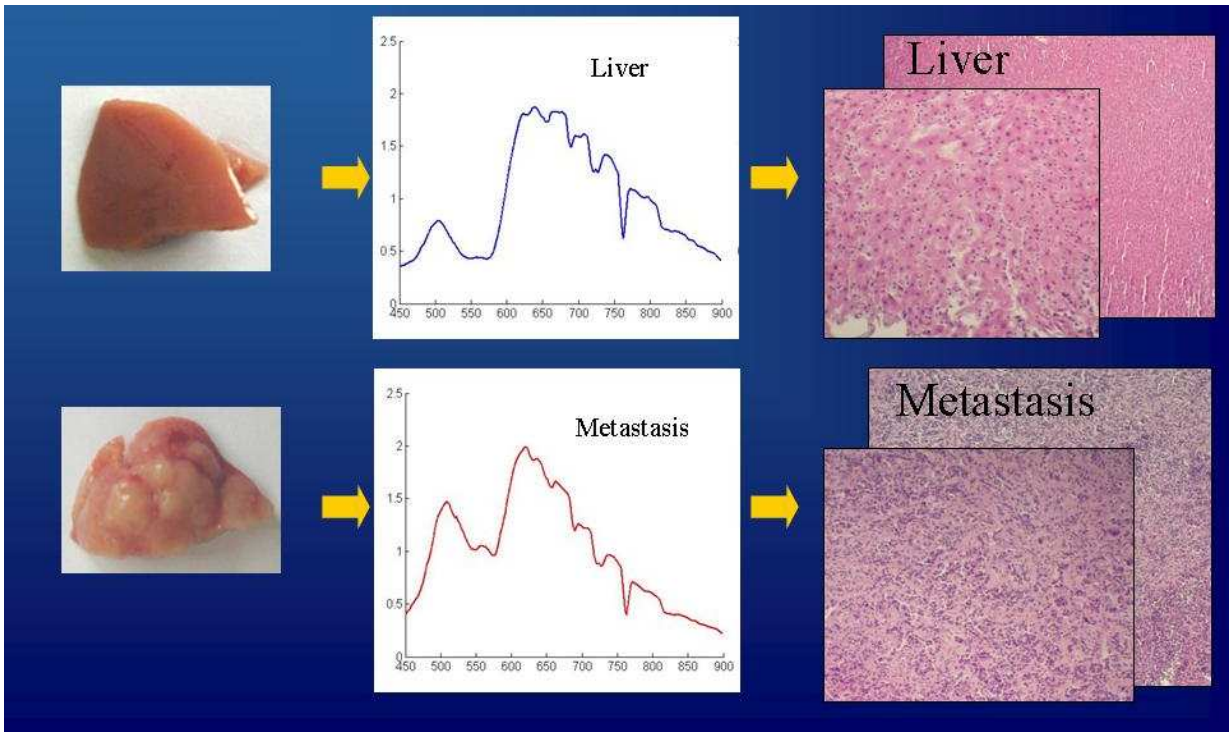

Fig. 4. Agreement of spectroscopic analysis (centre) and pathologic findings (right) in corresponding areas.

Provided that, on the basis of these data, the liver metastases can be distinguished from the normal liver, a key point to be taken into account concerns the fact that this discrimination could in part be favoured by the different colours of the two areas (liver > purple, metastases > white) and determined by a differential absorbance of the incident light. In other words, it is plausible that a consistent fraction of the diagnostic capability could depend on such differences, rather than the morphological and/or molecular peculiarities, being the measured reflectance complementary to the absorbance (19). The impact of such potentially confounding factor was investigated *in vivo*, as described in the following section.

***In vivo* analysis**

In order to test the diagnostic capability of the device in a pre-clinical trial situation, the comparative analysis, performed as described above, was repeated on a total of 50 anaesthetised rats.

Fig. 5 shows the average spectra and the standard deviation of the healthy liver and the metastatic counterpart.

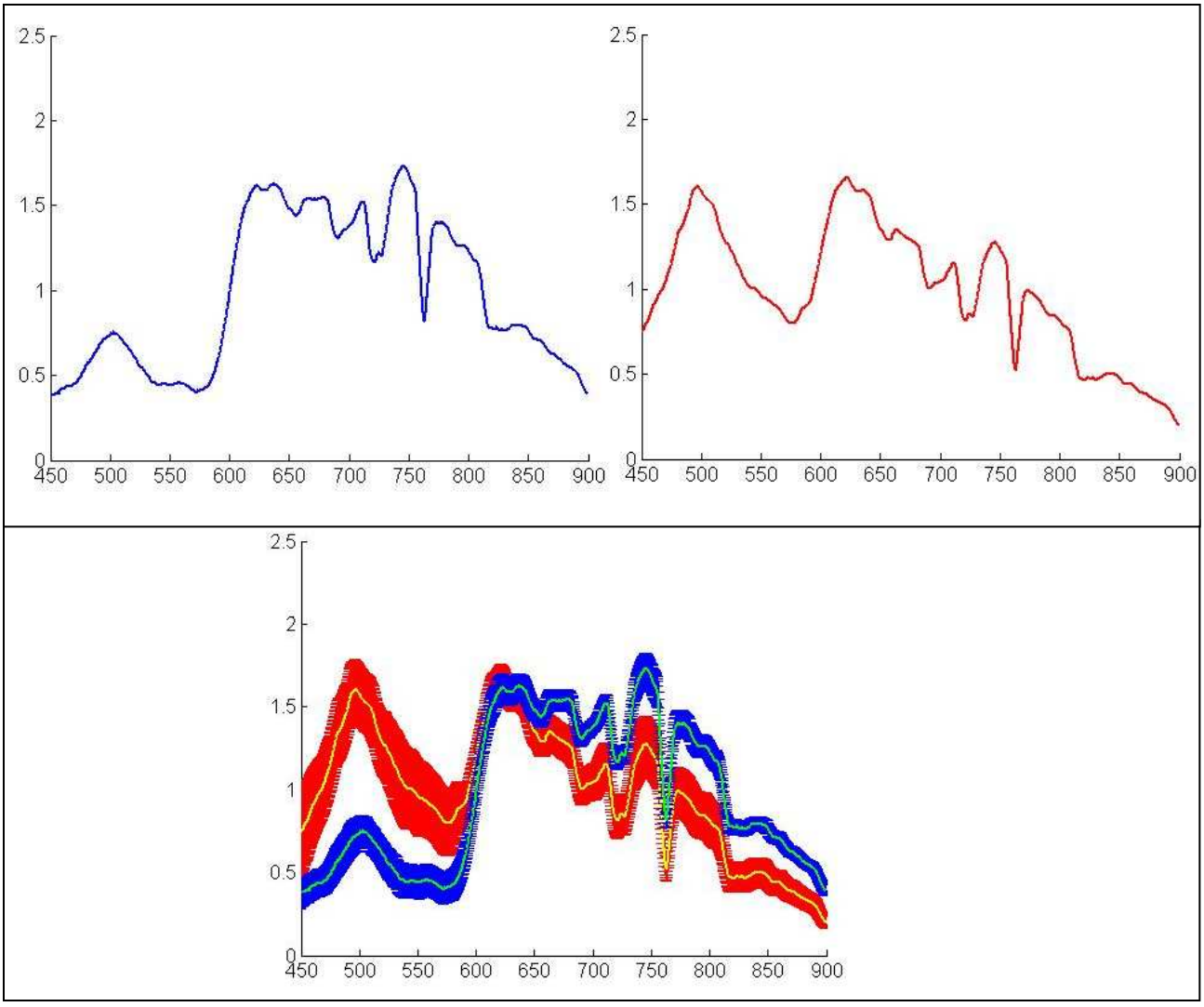

Fig. 5. Top panels: the 'average' spectra obtained after *in vivo* measurements of healthy liver (blue) and the metastatic counterpart (red).
Bottom panel: the average spectra shown on top are merged and the standard deviation shown. Blue: liver; red: metastasis.
Horizontal axis: wavelength values in nm; vertical axis: reflectance intensity expressed in arbitrary units.

As for the *ex vivo* situation, the reflectance intensities revealed consistent differences in particular intervals (e.g., 460 ÷ 580 nm, 690 ÷ 710 nm 780 ÷ 810 nm and 820 ÷ 880 nm) (fig. 2).

Also the approach regarding the spectra profile (fig. 6a-b) reveals several intervals where the differences between the healthy and the metastatic tissue appear significant with a confidence level (c. l.) of 95% at least.

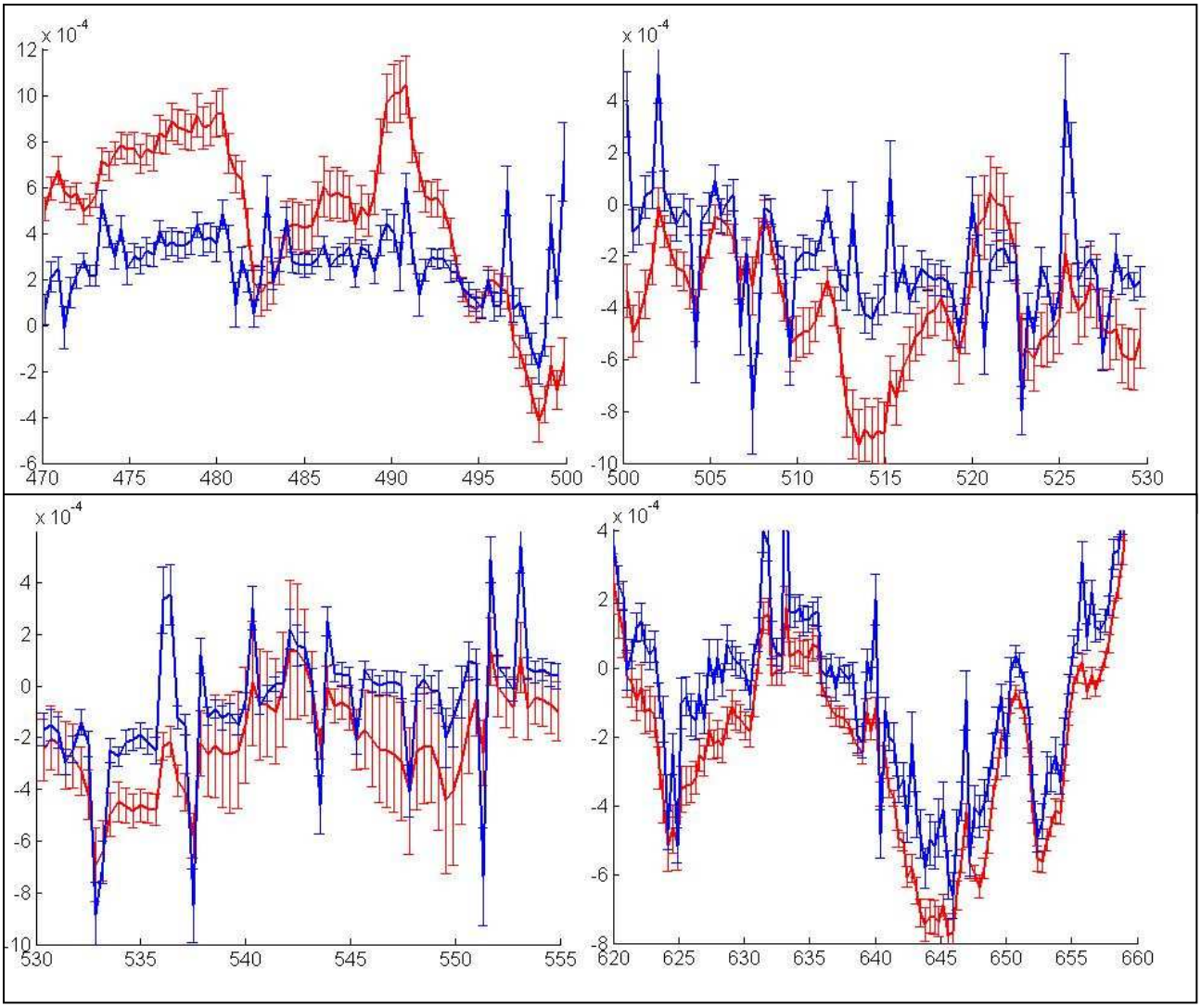

Fig. 6a. Comparison of (the approximation of) the first derivative of the curves shown in fig. 5. Blue: liver; red: metastasis. Wavelength intervals: 470 - 555 nm and 620 – 660 nm.
Horizontal axis: wavelength values in nm; vertical axis (exponential factors arise from the scaling of the diagrams): 'slope' of the respective part of the diagram shown in fig. 5.
Values above 0 correlate with ascending values of the reflectance, values below 0 correlate with descending values, while 0 indicates flat portions of the spectrum.

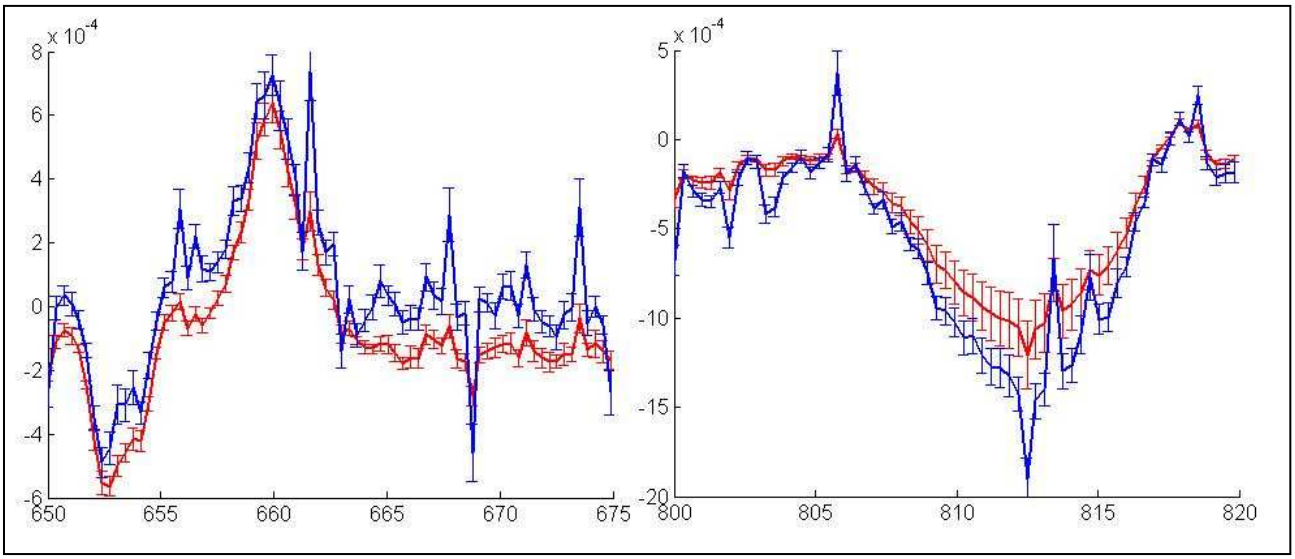

Fig. 6b. Comparison of (the approximation of) the first derivative of the curves shown in fig. 5. Blue: liver; red: metastasis. Wavelength intervals: 650 - 675 and 800 - 820 nm.
Horizontal axis: wavelength values in nm; vertical axis (exponential factors arise from the scaling of the diagrams): 'slope' of the respective part of the diagram shown in fig. 5.
Values above 0 correlate with ascending values of the reflectance, values below 0 correlate with descending values, while 0 indicates flat portions of the spectrum.

Similarly to the *ex vivo* session, the pathologic examination performed on the scanned specimens revealed differences in the tissue typology consistent with the spectroscopic data (fig. 7).

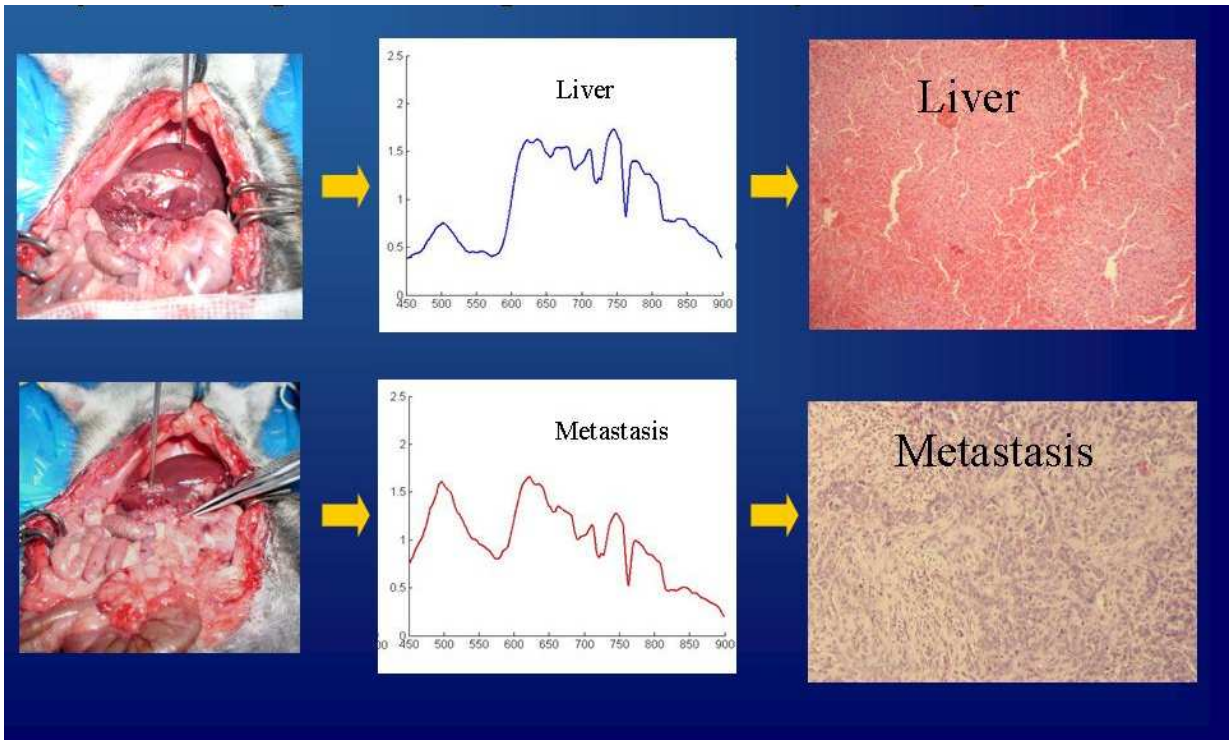

Fig. 7. Agreement between the spectroscopic analysis (centre) and the pathologic findings (right) of corresponding areas.

Several differences were found when the spectra and the trends of first derivative (spectral shape) of each tissue (liver, metastasis), as obtained from the *ex vivo* and the *in vivo* sessions, respectively, were compared (fig. 8a-b).

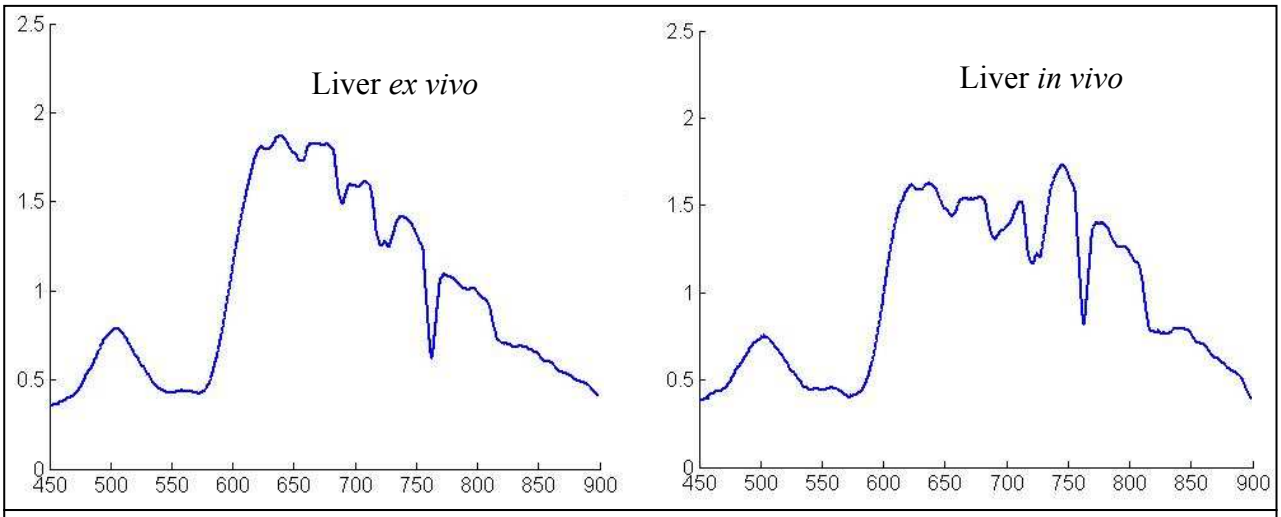

Fig. 8a. Comparison of spectra obtained from liver in the *ex vivo* and *in vivo* sessions.

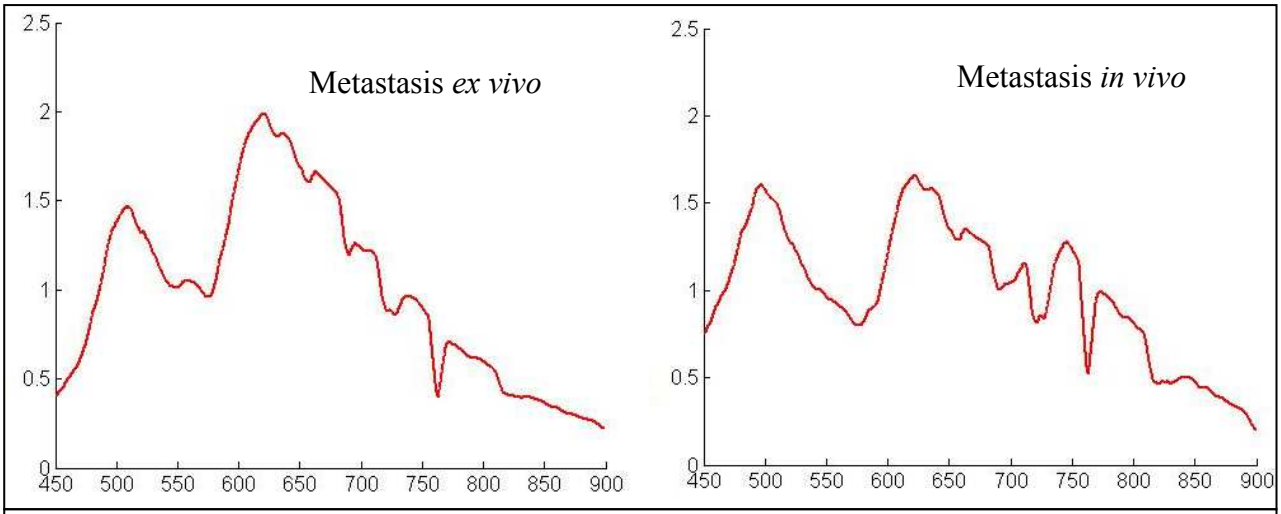

Fig. 8b. Comparison of spectra obtained from metastasis in the *ex vivo* and *in vivo* sessions.

For this reason the panel of the candidate diagnostic wavelengths was prudentially restricted to the significant differences shared by both the *ex vivo* and the *in vivo* sessions (c. l. ≥ 95%) and includes the following intervals: 470 ÷ 480 nm, 485 ÷ 495 nm, 626 ÷ 632 nm and 636 ÷ 640 nm, in addition to smaller intervals centred at about 500 nm and 535 nm, respectively.

At the moment we cannot explain definitively this differential response.

We assessed whether the neoplastic cells injection procedure could be responsible for this effect.

During an additional experimental session, sets of spectra were obtained from the liver of rats that did not undergo the intra-splenic injection of neoplastic cells, or received an injection of the sole medium (mock) where usually the cells are resuspended.

The spectral features of the non contaminated liver (not shown) confirmed the differences between the *ex-vivo* and *in vivo* context, already observed after the intra-splenic injection.

Given this result, significant changes in the optical properties may be attributed to the phenomena following tissue explantation (e. g., blood stasis, ischaemia …).

Taken altogether, the data confirmed that the diagnostic capability of the instrument was not impaired.

During the *in vivo* session, areas of connective tissue (liver hilum, omentum, surgical adherence) were investigated and the respective spectra recorded in parallel to those obtained from the metastases, then subjected to the usual mathematical approaches (fig. 9, 10, 11a-b).

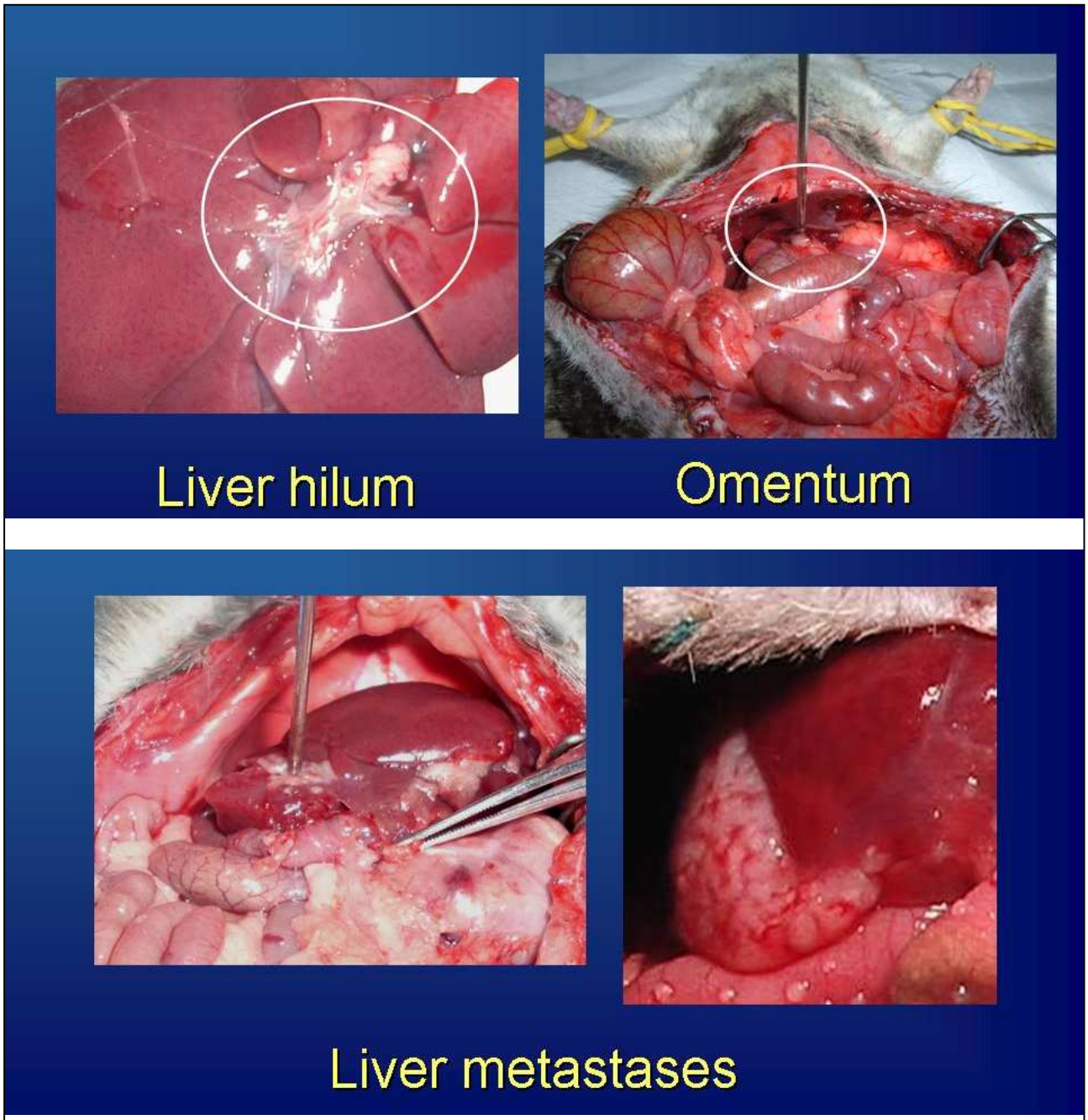

Fig. 9. Comparison of macroscopic feature of connective tissue (top) and liver metastases (bottom).

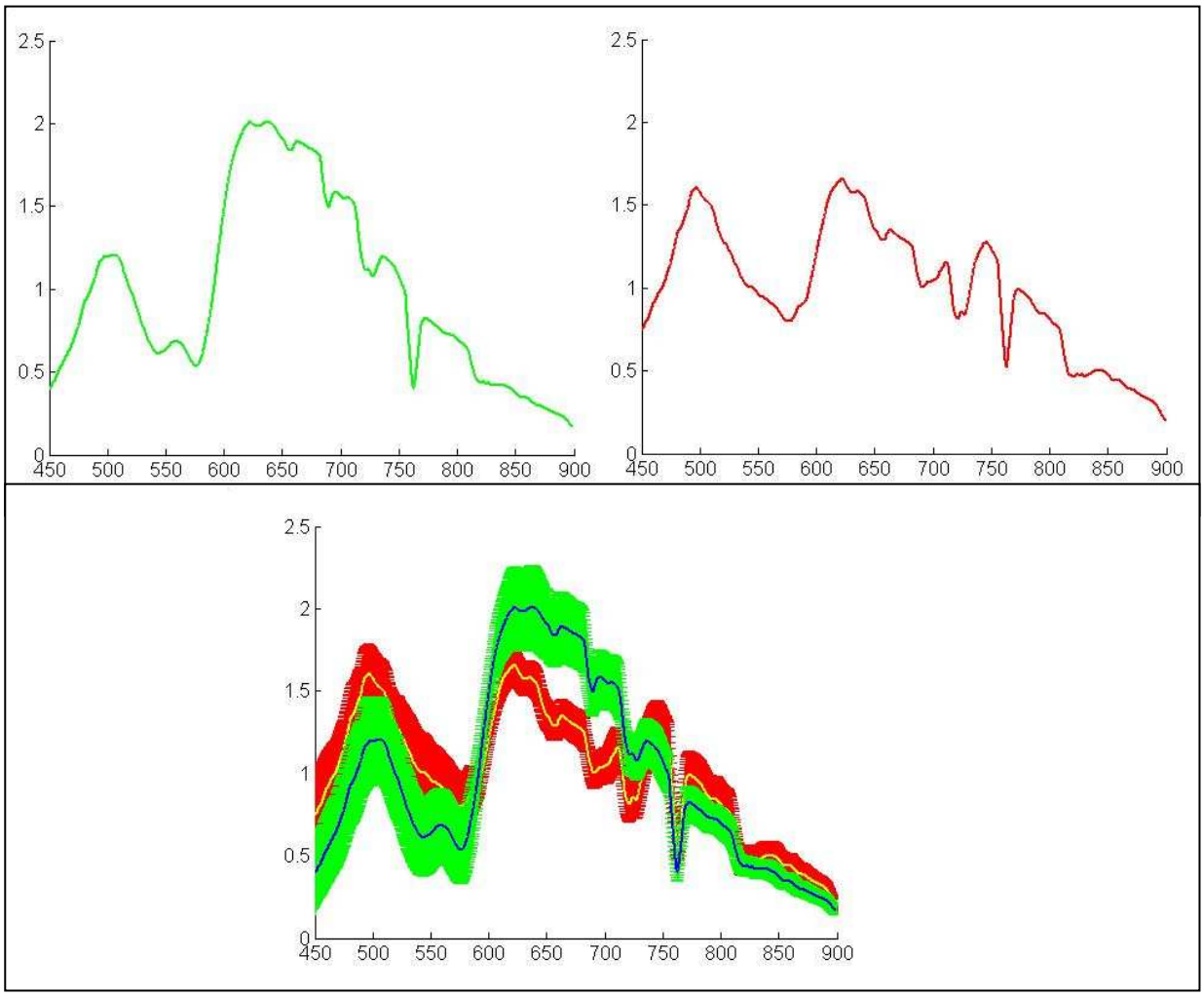

Fig. 10. Top panels: the 'average' spectra obtained after *in vivo* measurements of connective tissue (light green) and the metastatic counterpart (red).

Bottom panel: the average spectra shown on top are merged and the standard deviation shown. Light green: connective tissue; red: metastasis.

Horizontal axis: wavelength values in nm; vertical axis: reflectance intensity expressed in arbitrary units.

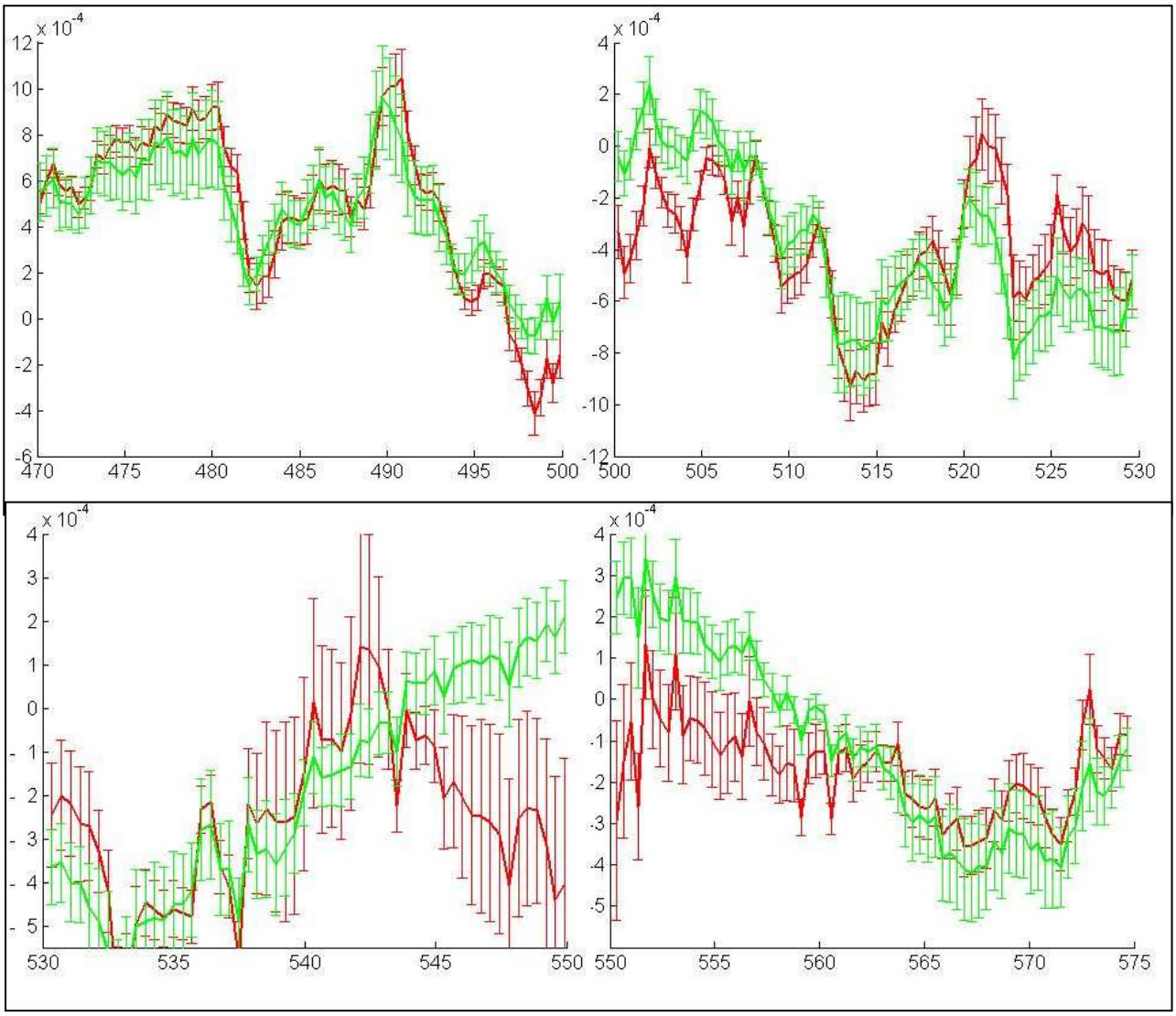

Fig. 11a. Comparison of (the approximation of) the first derivative of the curves shown in fig. 10.
Light green: connective tissue; red: metastasis. Wavelength interval: 470 – 575 nm.
Horizontal axis: wavelength values in nm; vertical axis (exponential factors arise from the scaling of the diagrams): 'slope' of the respective part of the diagram shown in fig. 10.
Values above 0 correlate with ascending values of the reflectance, values below 0 correlate with descending values, while 0 indicates flat portions of the spectrum.

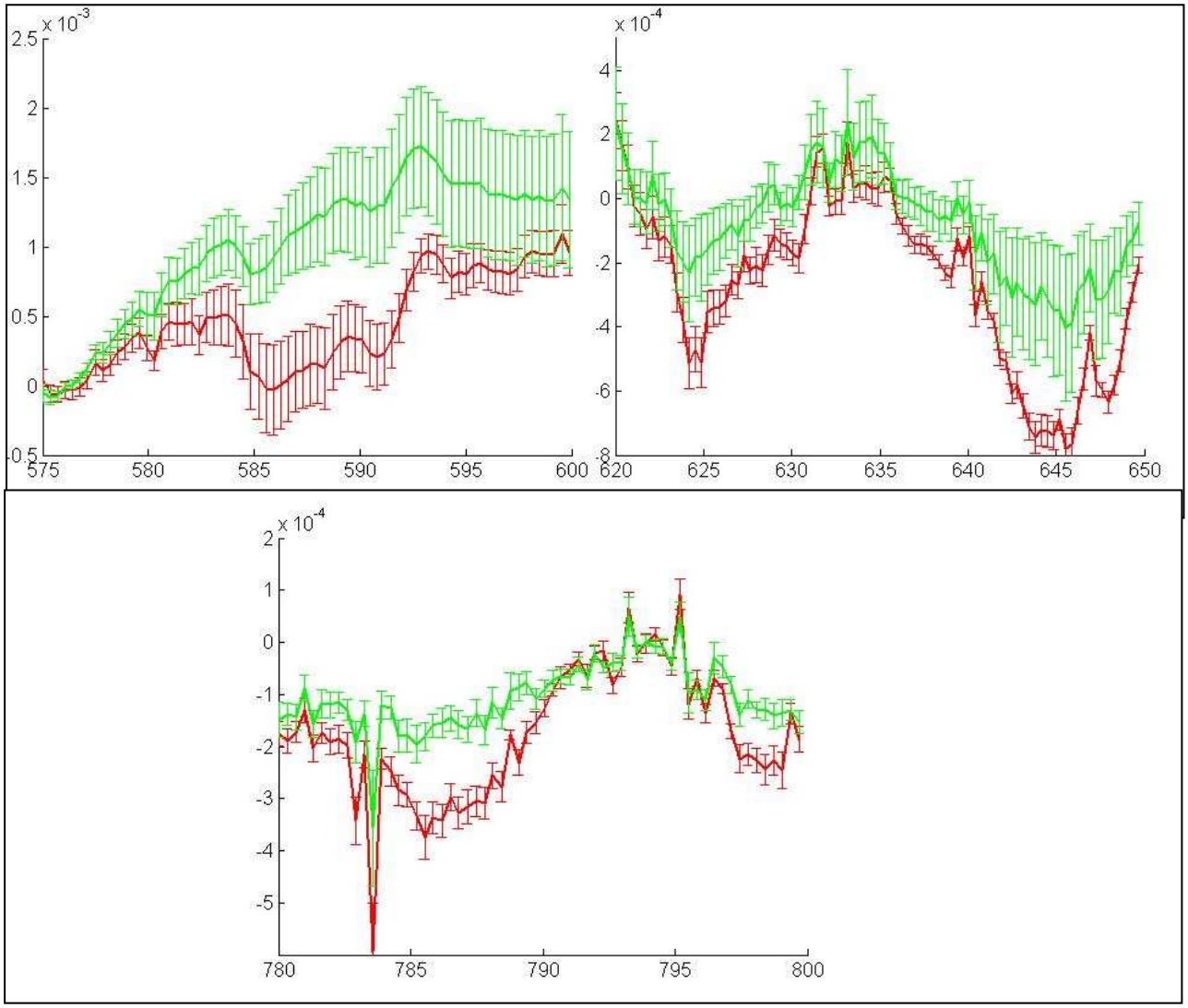

Fig. 11b. Comparison of (the approximation of) the first derivative of the curves shown in fig. 10.
Light green: connective tissue; red: metastasis. Wavelength intervals: 575 - 600nm, 620 - 650 nm and 780 – 800 nm.
Horizontal axis: wavelength values in nm; vertical axis (exponential factors arise from the scaling of the diagrams): 'slope' of the respective part of the diagram shown in fig. 10.
Values above 0 correlate with ascending values of the reflectance, values below 0 correlate with descending values, while 0 indicates flat portions of the spectrum.

Following the identification of several wavelength intervals, where the distinction between the connective tissue and the metastasis can be made with a confidence level of at least 95%, we conclude that the diagnostic capability of the instrument is not impaired by the presence of the connective tissue.

Once again, the different histological characteristics corresponded to the results of the spectroscopic analysis (fig. 12).

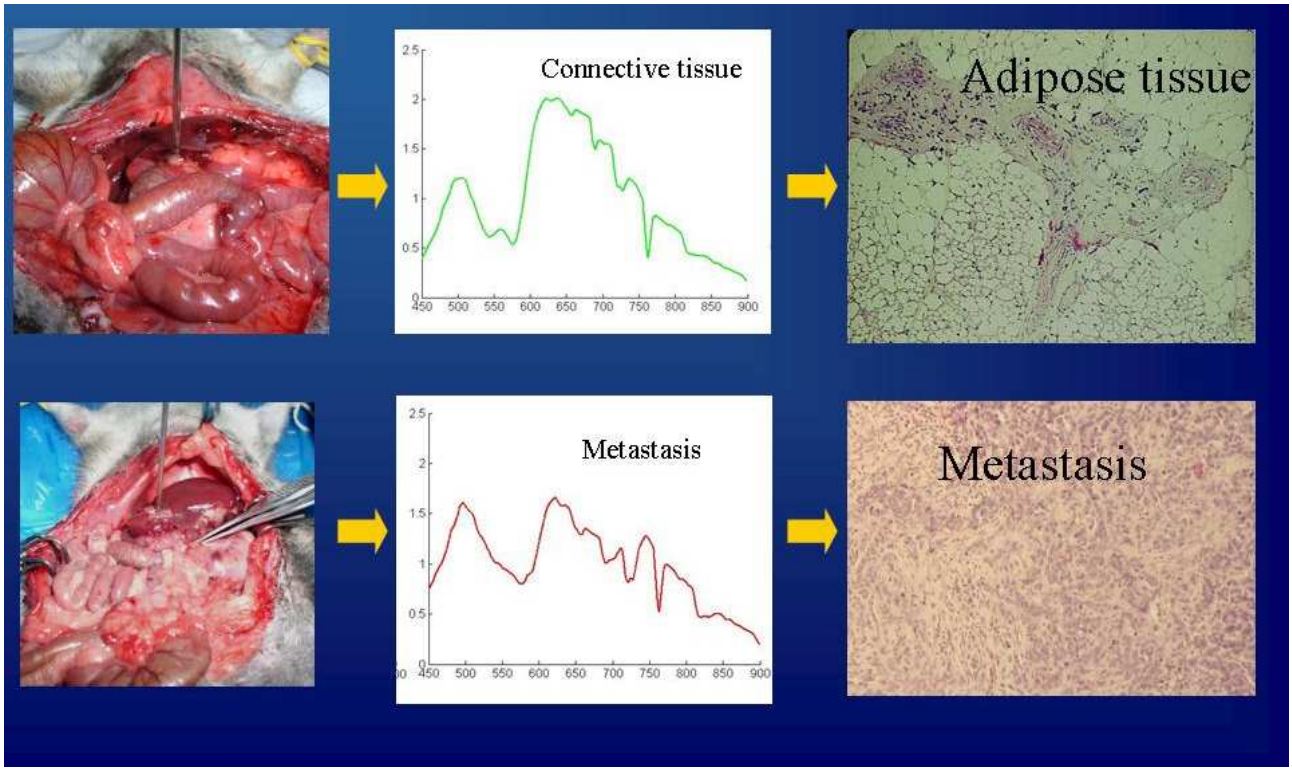

Fig. 12. Agreement between the spectroscopic analysis (centre) and microscopic findings (right) of corresponding areas.

These data indicate that the instrument is sensitive to the different molecular and morphological peculiarities of each anatomical district, so this approach based on

the DRS goes beyond the information merely based on the differences of colour that were almost negligible under specific experimental conditions.

LSS CONFIGURATION

Even if the LSS signal was correctly detected during a preliminary test on tissue phantom (p. 25), the periodic oscillations typical of the single scattering effect were not clearly detectable during *ex vivo* and *in vivo* analysis.

Thus, the LSS configuration was not as well informative for the diagnosis, that was rather based on the results of DRS approach.

DISCUSSION

The present study was aimed at determining whether an analytical approach complementary to LSS, namely based on the DRS, could be valid for distinguishing between the healthy and the metastatic portions of the rat liver in a *in vivo* simulated surgical procedure. The experiments were based on the preliminary use of an animal model, where the metastases can be confined in an anatomical site that allows for the simultaneous and specific recording of the diffuse reflectance spectra from the healthy, the metastatic and the connective tissue, respectively. The significance of the analytical approach relies on a consistent number of recorded data. Indeed, the spectra were analysed upon being chosen through a random number generator and the tissues could be differentiated, following either *ex vivo* or *in vivo* independent experimental sessions. In particular, the validation of the *in vivo* data reveals that several wavelength intervals may be crucial for the diagnostic capability of the instrument configuration adopted for these experiments. Although the identification of the intervals including the diagnostic wavelengths was limited on the basis of common features, shared by the *ex vivo* and *in vivo* data, respectively, the results so far produced put in evidence a specific response to the pathological condition, so that the instrument configuration appears reliable from a diagnostic point of view. According to what has been already reported in the literature about an analogous approach for the diagnosis of the breast cancer (14), our future experiments should be conceived in terms of the most appropriate ex-ante analysis: data collected from multiple experimental sessions should contribute to a

spectral classification based on the artificial intelligence pattern recognition, aimed at the assignment of parameters indicating the sensitivity and the specificity of our instrument.

The configuration of the probe used for the experiments described above is substantially equal to the instrumentation tested by Amelink (15).

This author tested a tissue phantom consisting of polystyrene spheres of different diameters by means of the visible light. Therefore, our configuration was expected to be suitable as well for discriminating the possible variations of the nuclear diameter, such as in the case of the neoplastic cells accumulation

Even if the LSS signal was correctly detected during a preliminary test upon tissue phantom, the periodic oscillations typical of the single scattering effect were not found out during either the *ex vivo* or the *in vivo* analysis in our model.

As reported by Perelman and collaborators (3), the data generated by means of the Mie scattering could be used in order to detect cancerous or even precancerous lesions, on the basis that the epithelial nuclei determine a periodicity in the reflectance, its amplitude being a function of size and number of nuclei.

However, the results from the tissue specimens examined by means of this methodology failed to prove clearly the existence of the periodic oscillations typical of the single scattering effect (even upon analysing different organs, such as mammary tissue and lung).

As far as the liver is concerned, the failure of the LSS may be justified by the controversial identification of the nuclei as the main scattering centres (10).

Apart from our experiments, it is conceivable that the experimental condition based on the LSS could be less appropriate for the examination of the biological tissue in general; indeed, at the time of our experiments, three subsequent articles, published from the same team that had first reported about the experimentation of LSS on the tissue phantom, showed data obtained from biological models and based rather on the differential path length spectroscopy (DPS) (4, 20, 21).

In all these recent articles the attention is mainly concentrated on the optical properties of the biological tissue and do not focus on the dimensions of the scattering centres; a convincing validation of the DPS approach emerged from these reports, at least for the cases of malignant lesions of the bronchial and oral mucosae.

Our results, although obtained through an alternative technique (DRS) and from a different tissue, indicate as well that a metastatic lesion can be detected independently from the periodic oscillation of the reflectance profile.

In principle it cannot be excluded that our reflectance signal may include a periodic fine structure component that could account for a very low percentage of the total signal, but the predominant phenomena could likely concern the absorption of the haemoglobin and the scattering effect produced by the collagen fibers, as already described in the literature (3).

These two chromophores generally determine a consistent signal, that can be neglected upon the application of the Monte Carlo simulations to specific models of light transport based on the Mie scattering (1, 22).

On the other hand, the haemoglobin concentration, its saturation degree, the blood vessels' density, the lipid and the collagen content of the tissue have been proven to be as well informative parameters for a pathological situation (23), like in the instance of cancerous lesions (4, 20, 21).

In the present study the main purpose has been that of developing a relatively economic instrument, with the potentiality of being a real-time diagnostic tool to be used during surgical interventions, rather than being optimised *a priori* for the identification of the sub-cellular structures responsible for the spectral features at specific wavelengths; yet the data obtained so far clearly show that the optical properties related to the tissue composition play an important role, given the capability of the instrument to discriminate quite well the metastatic from the connective tissue, though both show an almost equal appearance.

A deeper analysis of the possible influence of the haemoglobin on the results could be a valid starting point, since several spectra are characterised by a profile that, at least for a restricted wavelength interval (typically within 500 ÷ 600 nm), is strongly resembling the trend documented in the work of Backman and collaborators (24), that stressed about the presence of dips in such range, typically generated by the haemoglobin.

Our speculation derives from the observation that the spectra of the metastasis and the connective tissue show similar dips in that interval. Then the possibility of a differential response in relationship with a different metabolism of the heme (25) in the healthy hepatocytes with respect to the connective or the metastatic tissue

could be further investigated.

But before investigating on any molecular candidate, the results so far obtained in the animal model suggest that the same methodology should be worthy of being first exploited in humans affected by hepatic metastases, in order to confirm its reproducibility in a true clinical situation.

CONCLUSIONS

The results so far obtained put in evidence the good diagnostic accuracy of the device in tissue recognition (healthy liver, connective tissue, liver metastases) and the potentiality of being a real-time diagnostic tool to be used during surgical interventions.

The next step should be a clinical session aimed at the confirmation of the data reproducibility in a true intra-operative context (laparotomic or even laparoscopic).

REFERENCES

1. L.T. Perelman, J. Wu, I.I. Itzkan, M.S. Feld: Photon Migration in Turbid Media Using Path-Integrals. Phys. Rev. Lett., 72: 1341-1344, 1994.
2. A. Yodh, B. Chance: Spectroscopy and imaging with diffusing light. Phys. Today 48: 34-40, 1995.
3. L.T. Perelman, V. Backman, M. Wallace, G. Zonios, R. Manoharan, A. Nusrat, S. Shields, M. Seiler, C. Lima, T. Hamano, I. Itzkan, J. Van Dam, J.M.Crawford, M.S. Feld: Observation of Periodic Fine Structure in Reflectance from Biological Tissue: A New Technique for Measuring Nuclear Size Distribution. Phys. Rev. Lett. 80: 627-630, 1998.
4. A. Amelink, H.J. Sterenborg, M.P. Bard, S.A. Burgers: In vivo measurement of the local optical properties of tissue by use of differential path-length spectroscopy. Opt. Lett.: 29, 1087-1089, 2004.
5. R. Dukor: *Handbook of Vibrational Spectroscopy*, edited John Wiley & Sons Ltd., 2002.
6. H.C. vd Hulst: *Light scattering by small particles*, edited John Wiley, New York, 1957.
7. J.R. Mourant, A.H. Hielscher, A.A. Eick, T.M. Johnson, J.P. Freyer: Evidence of intrinsic differences in the light scattering properties of tumorigenic and nontumorigenic cells. Cancer Cytopathology: 84, 366-374 (1998).
8. J.R. Mourant, M. Canpolat, C. Brocker, O. Esponda-Ramos, T.M. Johnson, A. Matanock, K. Stetter, J.P. Freyer: Light scattering from cells: the contribution of the nucleus and the effects of proliferative status. J. Biomed. Opt.: 5, 131-

137, 2000.

9. B. Beauvoit, S.M. Evans, T.W. Jenkins, E.E. Miller, B. Chance: Correlation between the light scattering and the mitochondrial content of normal tissues and transplantable rodent tumors. Anal. Biochem.: 226, 167-174, 1995.
10. B. Beauvoit, B. Chance: Time resolved spectroscopy of mitochondria, cells and tissues under normal and pathological conditions Mol. Cell. Biochem.: 184, 445-455, 1998.
11. J.R. Mourant, I.J. Bigio, J. Boyer, R.L. Conn, T. Johnson, T. Shimada: Spectroscopic diagnosis of bladder cancer with elastic light Scattering. Lasers Surg. Med.: 17, 350-357, 1995.
12. J. Mourant, I. Bigio, J. Boyer, T. Johnson, J. Lacey: Elastic scattering spectroscopy as a diagnostic tool for differentiating pathologies in the gastrointestinal tract: preliminary testing. J. Biomed. Opt.: 1, 192 – 199, 1996.
13. Z. Ge, K. Schomacker, N. Nishioka.: Identification of colonic dysplasia and neoplasia by diffuse reflectance spectroscopy and pattern recognition technique. Appl. Spectrosc.: 52, 833-845, 1998.
14. I.J. Bigio, S.G. Bown, G. Briggs, C. Kelley, S. Lakhani, D. Pickard, P.M. Ripley, I.G. Rose, C. Saunders: Diagnosis of breast cancer using elastic-scattering spectroscopy: preliminary clinical results. J. Biomed. Opt.: 5, 221-228, 2000.
15. A. Amelink, M.P. Bard, S. Burgers, H.J. Sterenborg: Single-scattering spectroscopy for the endoscopic analysis of particle size in superficial layers of

turbid media. Appl. Opt.: 42, 4095-4101, 2003.

16. A. Caignard, M.S. Martin, M.F. Michel, F. Martin: Interaction between two cellular subpopulations of a rat colonic carcinoma when inoculated to the syngeneic host. Int. J. Cancer: 36, 273-279, 1985.
17. B. Chauffert, T. Shimizu, A. Caignard, A. Hammann, P. Genne, H. Pelletier, M.S. Martin: Use of a specific monoclonal antibody for studying the liver metastatic invasion of a rat colon cancer. In Vivo: 2, 301-305, 1988.
18. J.D. Bancroft, A. Stevens, *Theory and practice of histological techniques* 4th edn., edited Churchill Livingstone, New York, 1996.
19. W. Jacob, A. von Keudell, T. Schwarz-Selinger: Infrared analysis of thin films: amorphous, hydrogenated carbon on silicon, Brazilian Journal of Physics: 30, 508-516, 2000.
20. R.L. van Veen, W. Verkruysse, H.J. Sterenborg H.J: Diffuse-reflectance spectroscopy from 500 to 1060 nm by correction for inhomogeneously distributed absorbers. Optics Letters: 27, 246-248, 2002.
21. A. Amelink, O.P. Kaspers, H.J. Sterenborg., J.E. van der Wal, J.L. Roodenburg, M.J. Witjes: Non-invasive measurement of the morphology and physiology of oral mucosa by use of optical spectroscopy. Oral Oncol. : 44, 65-71, 2007.
22. J. Wu, M.S. Feld, R.P. Rava: Analytical model for extracting intrinsic fluorescence in turbid media. Appl. Opt: 32, 3585-3595, 1993.
23. R.L. van Veen, A. Amelink, M. Menke-Pluymers, C. van der Pol, H.J.

Sterenborg: Optical biopsy of breast tissue using differential path-length spectroscopy. Phys Med Bio: 50, 257-2581, 2005.

24. V. Backman, R. Gurjar, K. Badizadegan, I. Itzkan, R.R. Dasari, L.T. Perelman, M.S. Feld: Polarized light scattering spectroscopy for quantitative measurement of epithelial cellular structures in situ. Journal of Selected Topics in Quantum Electronics: 5, 1019-1026, 1999.
25. H. Fujita, J. Tohoku: Molecular Mechanisms of Heme Biosynthesis. Exp. Med.: 183, 83-99, 1997.

ACKNOWLEDGEMENTS

Dr. Riccardo Priore, University of Trieste

Dr. Gian Luigi Carlini, University of Trieste

Dr. Mauro Prasciolu, TASC-INFM, AREA Science Park, Trieste

Dr. Massimo Tormen, University of Trieste

Dr. Ubaldo Prati, Campanella Foundation - Institute of Cancer, Catanzaro

Prof. Fernando Tommasini, University of Trieste

Dr. Maria Assunta Cova, Cattinara Hospital, Trieste

Prof. Sabrina Pricl, University of Trieste

Prof. Paolo Dionigi, University of Pavia

Dr. Cinzia Ferrari, University of Pavia

Dr. Cecilia Zonta, University of Pavia

Mrs Anna Maria Clerici, University of Pavia

Mrs Anna Boninella, University of Pavia

Dr. Annalisa Gaspari, University of Pavia